

A theoretical exploration of birhythmicity in the p53-Mdm2 network

Wassim Abou-Jaoude, Madalena Chaves, Jean-Luc Gouzé

▶ **To cite this version:**

Wassim Abou-Jaoude, Madalena Chaves, Jean-Luc Gouzé. A theoretical exploration of birhythmicity in the p53-Mdm2 network. [Research Report] RR-7406, INRIA. 2010. inria-00523270v2

HAL Id: inria-00523270

https://inria.hal.science/inria-00523270v2

Submitted on 18 Oct 2010

HAL is a multi-disciplinary open access archive for the deposit and dissemination of scientific research documents, whether they are published or not. The documents may come from teaching and research institutions in France or abroad, or from public or private research centers.

L'archive ouverte pluridisciplinaire **HAL**, est destinée au dépôt et à la diffusion de documents scientifiques de niveau recherche, publiés ou non, émanant des établissements d'enseignement et de recherche français ou étrangers, des laboratoires publics ou privés.



INSTITUT NATIONAL DE RECHERCHE EN INFORMATIQUE ET EN AUTOMATIQUE

A theoretical exploration of birhythmicity in the p53-Mdm2 network

Wassim Abou-Jaoudé – Madalena Chaves – Jean-Luc Gouzé

N° 7406

Octobre 2010



ISSN 0249-6399

INSTITUT NATIONAL
DE RECHERCHE
EN INFORMATIQUE
ET EN AUTOMATIQUE

INRIA

centre de recherche SOPHIA ANTIPOLIS - MÉDITERRANÉE

A theoretical exploration of birhythmicity in the p53-Mdm2 network

Wassim Abou-Jaoudé[1], Madalena Chaves[2], Jean-Luc Gouzé[3]

Thème : Observation, modélisation et commande pour le vivant
Equipe-Projet COMORE
Rapport de recherche n° 7406 – Octobre 2010 -36 pages

Abstract: Experimental observations performed in the p53-Mdm2 network, one of the key protein module involved in the control of proliferation of abnormal cells in mammals, revealed the existence of two frequencies of oscillations of p53 and Mdm2 in irradiated cells depending on the irradiation dose. Recently, Ouattara, Abou-Jaoudé and Kaufman proposed a 3-dimensional differential model showing birhythmicity, i.e. the coexistence between two stable oscillatory regimes for the same external conditions, to reproduce the two frequencies experimentally observed. Here we analyze the mechanisms at the origin of the birhythmic behaviour through a theoretical exploration of this differential model. Our approach is to approximate this 3-dimensional continuous non-linear model which is difficult to analyse into a 3-dimensional then 2-dimensional piecewise affine model. A first return map analysis can then be used to extract the basic mechanisms for the emergence of birhythmicity. Based on this analysis, an experimental strategy is proposed to test the existence of birhythmicity in the p53-Mdm2 network.

Keywords: birhythmicity - piecewise affine models – genetic and metabolic networks

[1] INRIA, project-team COMORE, 2004 Route des Lucioles, BP 93, 06902 Sophia Antipolis, France – wassim.abou_jaoude@inria.fr
[2] INRIA, project-team COMORE, 2004 Route des Lucioles, BP 93, 06902 Sophia Antipolis, France – madalena.chaves@inria.fr
[3] INRIA, project-team COMORE, 2004 Route des Lucioles, BP 93, 06902 Sophia Antipolis, France – jean-luc.gouze@inria.fr

Centre de recherche INRIA Sophia Antipolis - Méditerranée
2004, route des Lucioles, BP 93, 06902 Sophia Antipolis Cedex (France)
Téléphone : +33 4 92 38 77 77 — Télécopie : +33 4 92 38 77 65

Une exploration théorique de la birhythmicité dans le réseau p53-Mdm2

Résumé: des observations expérimentales portant sur le réseau p53-Mdm2, un des modules clef impliqués dans le contrôle de la prolifération des cellules cancéreuses chez les mammifères, ont révélé l'existence de deux fréquences d'oscillations de la p53 et de Mdm2 dans des cellules irradiées en fonction de la dose d'irradiation. Récemment, Ouattara, Abou-Jaoudé et Kaufman ont proposé un modèle différentiel à 3 dimensions présentant de la birhythmicité, un phénomène dynamique complexe caractérisé par la coexistence entre deux régimes oscillants pour des conditions extérieures identiques, pour reproduire les deux fréquences observées expérimentalement. Le but de ce travail est d'analyser les mécanismes qui sont à l'origine de l'émergence de phénomène birhythmique à travers une analyse théorique de ce modèle différentiel. Pour cela, nous avons approximé ce modèle continu et non-linéaire, difficile à analyser, en un modèle à 3 dimension puis à 2 dimension affine par morceaux. Une application de premier retour peut alors être calculée pour extraire les mécanismes à l'origine de la birhythmicité. A partir de cette analyse, une stratégie expérimentale est finalement proposée pour tester l'existence d'un phénomène birhythmique dans le réseau p53-Mdm2.

Mots clés: birhythmicité - modèles affines par morceaux – réseaux génétiques et métaboliques

1 Introduction

Periodic phenomena are encountered at all levels of biological organization, with periods ranging from fractions of a second to years [1]. At the intracellular level, periodic phenomena have been reported in various biochemical systems such as calcium signalling, circadian rythms, cell cycle, glycolysis, cAMP signaling in *Dictyostelium* [1,2] or the p53-Mdm2 network [3]. Most of the time, biochemical oscillations display a simple pattern with a single oscillatory regime of stable period and amplitude. However, rhythmic processes can sometimes present a more complex behavior. One mode of complex oscillatory behavior is the coexistence between two simultaneously stable oscillatory regimes for the same external conditions. This phenomenon, called birhythmicity [1,4], is the counterpart of bistability for oscillatory behaviors. Such a behavior has been observed in a number of chemical oscillatory systems [5,6] but, although some studies suggest its occurrence in the heart and the neuronal system [7], birhythmicity has not yet been firmly observed experimentally in biological systems.

Recent experiments performed in the p53-Mdm2 network, one of the key protein module involved in the control of proliferation of abnormal cells in mammals [8,9,10], reported two oscillatory regimes of p53 and Mdm2 in irradiated cells [11]: a low-frequency oscillatory regime at low irradiation dose with a period of about 10h and high-frequency oscillations at high irradiation dose with a period of about 6h (Figure 1). This observation raised the question of the existence of birhythmicity in the p53-Mdm2 network which would be at the origin of the two oscillatory regimes experimentally observed as a function of the irradiation dose.

A theoretical answer to this question has been recently brought by Ouattara, Abou-Jaoudé and Kaufman [12,13]. In the framework of a simple 3-dimensional differential model of the p53-network, they showed that this system could display birhythmicity for a certain range of irradiation dose [12]. Thanks to the presence of this birhythmic behavior, they could reproduce the two frequencies experimentally observed as well as the increase of the fraction of cells oscillating with a high frequency when the irradiation dose increases and the changes in the oscillation frequency in the course of the response that have been observed for some cells after irradiation [12,13].

Following this work, the aim of this paper is to investigate the mechanisms at the origin of the birhythmicity in Ouattara, Abou-Jaoudé and Kaufman's model (OAK model). As this 3-dimensional continuous non-linear differential model is difficult to analyze, we approximated it, in a first step, into a 3-dimensional piecewise linear differential model where the Hill functions have been replaced by step functions and, in a second step, into a 2-dimensional piecewise linear differential model by setting one variable as a constant in each domain of the phase space delimited by the thresholds of the step functions. Analyzing the dynamics of the system in the framework of a piecewise linear differential description allowed us to reveal the phase space structure of the two oscillatory regimes composing the birhythmic behavior.

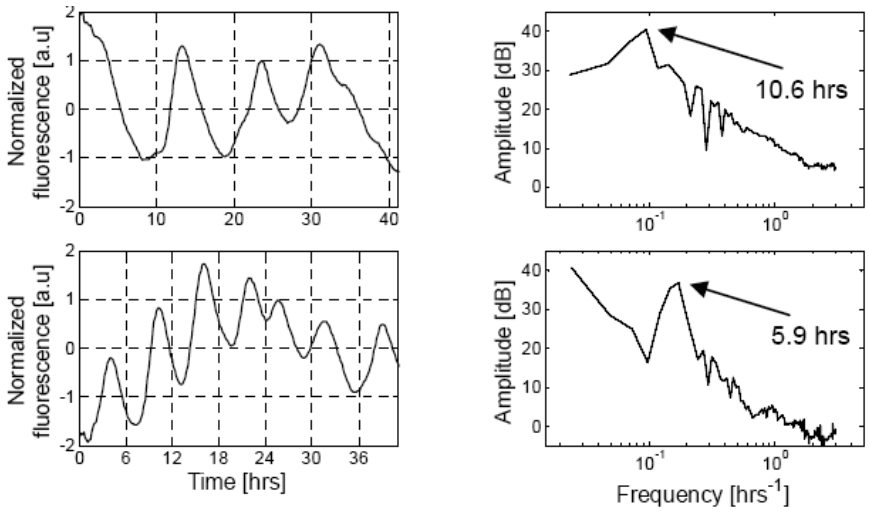


Figure 1. Experimental data from (Geva-Zatorsky et al., 2006, Fig.S3) [11]. Power spectrum of nuclear Mdm2-YFP fluorescence dynamics in individual cells. Top: an example of a cell showing fluctuations with a characteristic frequency of ~10 hours (exposed to 0.3Gy of gamma irradiation), and the power spectrum of the signal (by Fourier transform). Bottom: an example of a cell with multiple oscillations with a period of ~6 hours (exposed to 5Gy), and the power spectrum of the signal (right). Reprinted by permission from Macmillan Publishers Ltd: Molecular Systems Biology, advance online publication, 2006 (doi: 10.1038/msb4100068).

Following this analysis, we find that two features related to the phase space structure of the system are at the origin of birhythmicity observed in the OAK model: (1) the existence of two embedded cycles in the transition graph of the piecewise differential models; (2) the presence of a bypass containing two folds in the orbit of the large amplitude oscillatory regime of low frequency. Calculation of a first return map further permitted to give an interpretation of the role of these two features in the emergence of the birhythmic phenomenon. Finally, from this analysis, an experimental strategy is proposed to test the existence of birhythmicity in the p53-Mdm2 network.

2 Results

2.1 Birhythmicity in the OAK Model

The model of the p53-Mdm2 core network proposed by Ouattara, Abou-Jaoudé and Kaufman is a three-variable model, inspired by the work of Ciliberto et al. [14], which describes the interaction between p53, cytoplasmic Mdm2 and nuclear Mdm2. We briefly recall the biological data from which this model has been elaborated (see [12], for a more detailed description). Nuclear Mdm2 down regulates p53 by accelerating its degradation through ubiquitination [15-17] and by blocking its functional activity [18-20]. p53 up regulates cytoplasmic Mdm2 level by enhancing the transcription of gene *MDM2* [21,22]. p53 inhibits the translocation of Mdm2 from the cytoplasm to the nucleus [23]. These interactions are summarized by the influence diagram shown in Figure 2. Importantly, the degradation rate of nuclear Mdm2 (d_{Mn}) depends on DNA damage caused after cell irradiation [24,25] and increases when DNA damage increases [13].

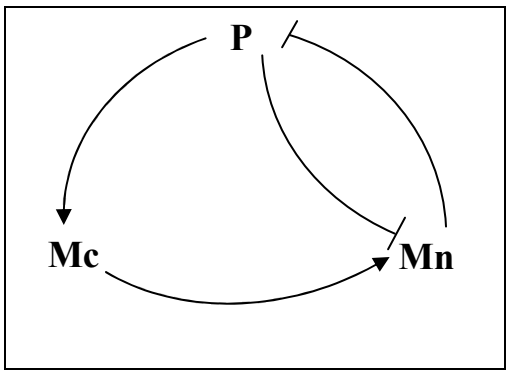


Figure 2. Schematic representation of the p53-Mdm2 core network. Normal arrows correspond to positive interactions, blunt arrows to negative interactions. P, Mc and Mn represent p53, cytoplasmic Mdm2 and nuclear Mdm2 respectively.

To describe the dynamics of this network, Ouattara, Abou-Jaoudé and Kaufman built a three-dimensional differential model (which will be called the OAK Model for the following) to represent the temporal evolution of the level of p53, cytoplasmic and nuclear Mdm2. We recall the equations of the OAK Model in Text S1. For appropriate parameter values, a bifurcation analysis of this model as a function of d_{Mn} showed the existence of a domain of birhythmicity separating two oscillatory regimes of different amplitude, period and mean values (see Figure 2b in [13], and Figure S1) which allowed to reproduce the two characteristic periods of p53 oscillations observed experimentally by Geva-Zatorsky et al. as a function of cell irradiation dose (Figure 1).

2.2 A three-dimensional reduced model

Starting from the OAK model, we firstly performed an analysis of the influence of the different terms involved in the equations of this model to see if some of them had no significant influence on the oscillatory dynamics of the system, in particular on the birhythmic behavior. Our analysis suggests that the terms modeling the translocation process of Mdm2 from the nucleus to the cytoplasm and the bilinear term modeling Mdm2-mediated acceleration of p53 degradation would have little influence on the oscillatory dynamics (see Text S2). Suppressing these terms, the OAK Model becomes:

$$\frac{\mathrm{d}P}{\mathrm{d}t} = k_P \frac{K_P^n}{K_P^n + Mn^n} - d_P \cdot P$$

$$\frac{\mathrm{d}Mc}{\mathrm{d}t} = k_{Mc} + k'_{Mc} \frac{P^n}{K_{Mc}^n + P^n} - \left(k_{in} - k'_{in} \frac{P^n}{K_{Mn}^n + P^n} \right) \cdot Mc - d_{Mc} Mc$$

$$\frac{\mathrm{d}Mn}{\mathrm{d}t} = V_r \left(k_{in} - k'_{in} \frac{P^n}{K_{Mn}^n + P^n} \right) \cdot Mc - d_{Mn} Mn$$

(Model 1)

where P, Mc and Mn represent the concentration of p53, cytoplasmic Mdm2 and nuclear Mdm2 respectively.

Numerical simulations of Model 1 show that, for appropriate parameter settings, the bifurcation diagram as a function of d_{Mn} is very similar to the bifurcation picture of the OAK Model if the non-linearities (i.e. Hill coefficients n) are slightly increased (Figure 3A, and Figure S1A). As d_{Mn} increases, Model 1 displays successively a stable steady state with a low level of p53, the coexistence of this stable steady state with two unstable steady states, a stable oscillatory state, and finally a stable steady state with high levels of p53. In the oscillatory domain, Model 1 shows two limit cycles, a large amplitude oscillatory regime of low frequency for low d_{Mn} values and a small amplitude oscillatory regime of high frequency for high d_{Mn} values, separated by a birhythmic region where these two regimes coexist (Figure 3A). In the domain of birhythmicity, numerical simulations in the phase space moreover show that the phase portrait of the two limit cycles for the OAK Model is very similar to the one for Model 1 (Figure 3B, and Figure S1B). In the following of this work, Model 1 will thus be used as the starting model to investigate the mechanisms leading to the emergence of the birhythmic behavior in the OAK Model.

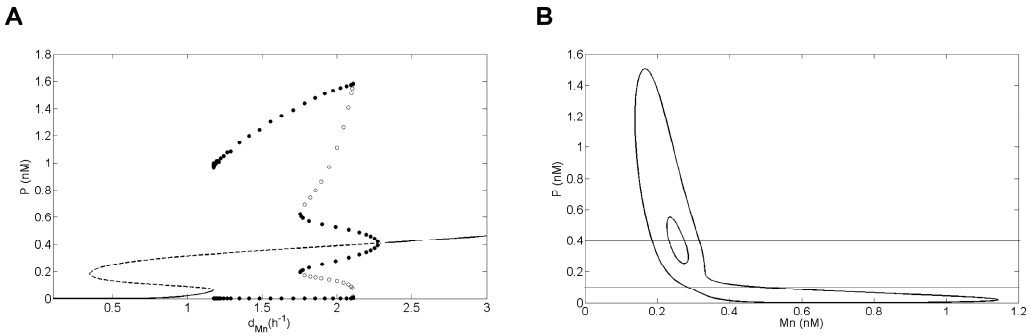


Figure 3. Bifurcation diagram and projection of the phase portrait of birhythmicity in the plane (Mn,P) for Model 1. (A) Bifurcation diagram of p53 level as a function of d_{Mn} for Model 1. Solid lines (resp. dotted lines) represent the stable (resp. unstable) equilibrium points. Bold (resp. white) dots are the maxima and minima of the stable (resp. unstable) limit cycles. The system shows a birhythmic domain for 1.75 h^{-1}<d_{Mn}<2.11 h^{-1}. (B) Projection of the two oscillatory regimes on the plane (Mn,P) for Model 1 for d_{Mn}=1.9 h^{-1}. The thresholds K_{Mc} and K_{Mn} related to P are indicated in solid lines. The parameter values of Model 1 are the same as for the OAK Model (K_{Mn}=0.1 nM) except: n=6, d_P=2.5 h^{-1} and K_{Mc}=0.4 nM (see legend of Figure S1 for the parameter values of the OAK Model).

We next qualitatively analyzed the main differences between the two oscillatory regimes for Model 1. Our analysis shows significant differences between the shape of the orbits of the two oscillatory regimes in the phase space (Figure 3B). Indeed:

- the small amplitude oscillatory regime of short period has a regular shape. Moreover, p53 level stands well above K_{Mn} threshold all along the trajectory of the cycle. The Hill function $\frac{P^n}{K_{Mn}^n + P^n}$ modeling the inhibition of Mdm2 translocation into the nucleus by p53 has thus no significant importance along this cycle ($\frac{P^n}{K_{Mn}^n + P^n} \approx 1$).

-on the contrary, the large amplitude oscillatory regime of long period contains a long "tail" in the phase space domain where p53 is below K_{Mn} threshold and its orbit crosses the two thresholds, K_{Mn} and K_{Mc}, related to P.

Finally, we performed an analytical study of the dynamics of the system by investigating general properties concerning the existence of limit cycles. Contrary to 2-dimensional differential systems where the Poincaré-Bendixson theorem gives general conditions for the existence of periodic orbits, there is no such equivalent theorem concerning the existence of periodic orbits for 3-dimensional differential system except for particular systems such as competitive or cooperative systems [26]. In the case of Model 1, an analysis of the sign of the elements of the Jacobian Matrix interestingly shows that this model is indeed equivalent to a competitive system (Text S3). According to Hirsch [27], a Poincaré-Bendixson theorem in dimension 3 holds. Moreover, for the parameter values for which the system displays birhythmicity, a numerical study of the equilibrium points suggests that there is only one equilibrium point which is unstable and for which the stable manifold is 1-dimensional (Text S3). Applying the Poincaré-Bendixson theorem for 3-dimensional competitive systems, it can be proved that the system admits a periodic orbit for the parameter values for which the system displays birhythmicity [26]. Under some supplementary assumptions which are here respected, we can moreover show that there exists a stable periodic orbit [28]. However, these theorems do not tell how many periodic orbits the system has and thus do not provide a mathematical proof of the existence of birhythmicity in our model.

2.3 From continuous to discrete model: approximation of the Hill functions to step functions

Although we can derive some general properties concerning the dynamics of the 3-dimensional differential Model 1, it is still difficult to get insight into more detailed information about the dynamics of the system, in particular about the birhythmic behavior. However, the equations of Model 1 involves several highly non-linear terms of the Hill form:

$$\Phi(X) = \frac{X^n}{\nu^n + X^n} \text{ for increasing Hill functions;}$$

$$\Psi(X) = \frac{\nu^n}{\nu^n + X^n} \text{ for decreasing Hill functions.}$$

We thus approximated Model 1 by replacing these terms by step functions with two levels (Figure 4):

$$s^+(X,\nu) = 0 \text{ if } X \le \nu$$
$$s^+(X,\nu) = 1 \text{ if } X \ge \nu$$

for increasing Hill functions and:

$$s^-(X,\nu) = 1 \text{ if } X \le \nu$$
$$s^-(X,\nu) = 0 \text{ if } X \ge \nu$$

for decreasing Hill functions, where ν represents now the threshold of the step functions. Such an approximation has been originally proposed by Glass and Kaufman [29] for biochemical networks and has been since widely used to model genetic systems [30-33].

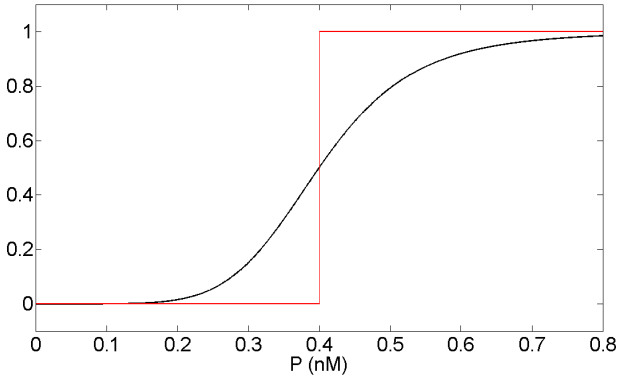


Figure 4. Approximation of Hill function to step function. Hill function $f(P)=\frac{P^n}{K_{Mc}^n+P^n}$ which appears in the equation of Mc in Model 1 (in black) and its approximation into the step function s^+ defined as: $s^+(P,K_{Mc})=0$ if $P<K_{Mc}$ and $s^+(P,K_{Mc})=1$ if $P>K_{Mc}$ (in red) for n=6 and K_{Mc}=0.4 nM. n is the Hill coefficient and characterizes the steepness of the Hill function.

This approximation leads to a piecewise linear differential model whose equations are:

$$\frac{dP}{dt}=k_P\cdot s^-(Mn,K_P)-d_P\cdot P$$
$$\frac{dMc}{dt}=k_{Mc}+k'_{Mc}s^+(P,K_{Mc})-\left(k_{in}-k'_{in}s^+(P,K_{Mn})\right)\cdot Mc-d_{Mc}Mc$$
$$\frac{dMn}{dt}=V_r\left(k_{in}-k'_{in}s^+(P,K_{Mn})\right)\cdot Mc-d_{Mn}Mn$$

(Model 2)

The space of variables can thus be decomposed into 6 domains (D^{11}, D^{21}, D^{12}, D^{22}, D^{13}, D^{23}) delimited by the threshold values of the step functions: K_P, K_{Mn} and K_{Mc} (Figure 5A). The equations of evolution in each domain of the phase space are detailed in Table S1. In each domain, the equations are affine and stable and one can calculate a so-called *target equilibrium point* of the domain towards which the system will tend (Table S2)[4]. If a target equilibrium point of a domain D does not belong to its domain, then the system starting from D will leave D at some point as it will reach sooner or later a boundary of the domain. If a target equilibrium point of a domain D belongs to D, it corresponds to a local equilibrium point of the system. Impor-

[4]The target equilibrium point is an analogous of the *focal point* defined in a class of piecewise linear diagonal models [34] (see next section).

tantly, the equation of Mn depends on Mc. It follows that the sign of the derivative of Mn can change in each domain of the phase space according to Mc[5].

For appropriate parameter settings, numerical simulations show that the bifurcation diagram as a function of d_{Mn} is similar to the bifurcation picture of Model 1: a stable steady state of low p53 values for low d_{Mn} values corresponding to the target equilibrium point of domain D^{21} (P=0, $Mc = \frac{k_{Mc}}{k_{in} + d_{Mc}}$, $Mn = \frac{V_r \cdot k_{in}}{d_{Mn}} \cdot \frac{k_{Mc}}{k_{in} + d_{Mc}}$), a stable steady state of high p53 levels for high d_{Mn} values corresponding to the target equilibrium point of domain D^{13} ($P = \frac{k_P}{d_P}, Mc = \frac{k_{Mc} + k'_{Mc}}{k_{in} - k'_{in} + d_{Mc}}$, $Mn = \frac{V_r (k_{in} - k'_{in})}{d_{Mn}} \cdot \frac{k_{Mc} + k'_{Mc}}{k_{in} - k'_{in} + d_{Mc}}$) and an oscillatory regime for intermediate d_{Mn} values (see Text S4 and Figure 6). In the oscillatory region, there exists an interval of d_{Mn} values in which the system displays birhythmicity with the coexistence of two oscillatory regimes of different amplitude and period (Figure 6):

- a small amplitude oscillatory regime of short period, crossing domains D^{12}, D^{22}, D^{13} and D^{23}, in which K_{Mn} threshold is not functional ($P>K_{Mn}$). This periodic orbit corresponds to the small amplitude oscillatory regime appearing in Model 1 (Figure 3);
- a large amplitude oscillatory regime of long period passing through all the domains of the phase space. This periodic orbit corresponds to the large amplitude oscillatory regime of Model 1 (Figure 3) and contains a "tail" located in domain D^{12}. As also observed for Model 1, this "tail" contains two folds where the sign of dMn/dt changes: a fold in the transition between D^{22} and D^{21} and a fold inside domain D^{21}.

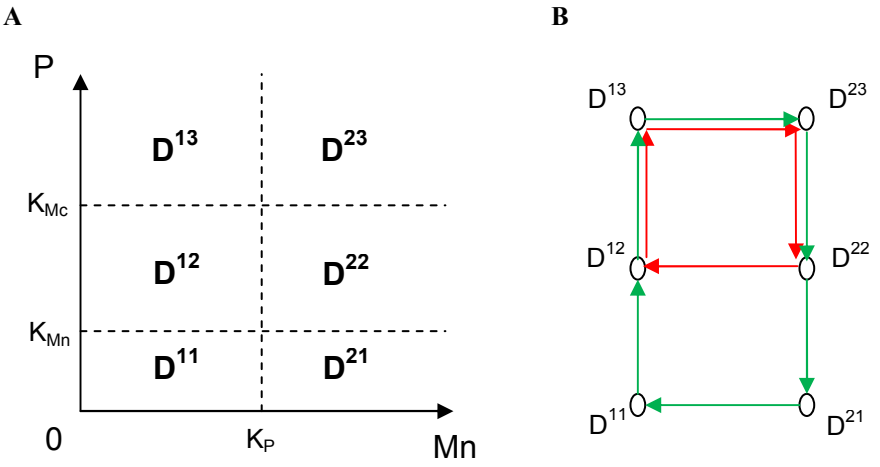


Figure 5. Subdivision of the phase space and graph of transitions for Model 2. (A) Subdivision of the phase space for Model 2 in 6 domains delimited by the thresholds K_P, K_{Mn} and K_{Mc}. (B) Graph of the transitions followed by the two oscillatory regimes composing birhythmicity shown in Figure 6. The small amplitude oscillatory regime of short period crosses D^{22}, D^{12}, D^{13} and D^{23} successively (in red). The large amplitude oscillatory regime of long period crosses domains: D^{22}, D^{21}, D^{11}, D^{12}, D^{13} and D^{23} successively (in green).

[5]The transition graph, which is the graph defining the possible transitions between the different domains [35], can thus not be directly derived from the position of the target equilibrium points (see next section).

The transitions between the different domains followed by the small and the large amplitude limit cycles are shown in Figure 5B. As emphasized in the previous section, the orbits of the two limit cycles are significantly different. Here, approximating the continuous Model 1 into a piecewise linear one allows to better understand the main qualitative differences between the two oscillatory regimes composing the birhythmic behavior as it enables decomposing the trajectory of the limit cycles into different steps and transitions between different dynamical regimes which can be biologically interpreted. Starting from the threshold delimiting domain D^{12} and D^{13} (i.e. p53 levels in its highest threshold K_{Mc} and nuclear Mdm2 levels is below its threshold K_P), the two oscillatory regimes can be described as follows. As p53 level goes above the K_{Mc} threshold, p53 starts to activate the expression of gene *MDM2* and thus the production of cytoplasmic Mdm2. Mdm2 is then translocated into the nucleus where it accumulates. When nuclear Mdm2 level gets beyond its threshold K_P, it starts to inhibit p53 activity (domain D^{23}). p53 level then decreases. As its level goes below its threshold K_{Mc}, p53 no longer activates the expression of *MDM2*. Cytoplasmic Mdm2 thus starts to decrease leading to a decrease of nuclear Mdm2 level (domain D^{22}). As p53 and nuclear Mdm2 levels both decrease, two alternatives can be taken by the system leading to either the small or the large amplitude oscillatory regime, which corresponds to the branching point in the graph of Figure 5B:

- either nuclear Mdm2 level first goes below its threshold K_P. Nuclear Mdm2 then no longer inhibits p53 and p53 level starts to increase again (domain D^{12}) until it reaches its threshold K_{Mc} which closes the trajectory of the small amplitude limit cycle.
- or p53 level first goes below its threshold K_{Mn}. p53 then no longer inhibits Mdm2 entry into the nucleus (domain D^{21}) and nuclear Mdm2 starts to rise again leading to the first fold observed in the large amplitude limit cycle. However, in the same time, cytoplasmic Mdm2 decreases because p53 level is too low to activate *MDM2* transcription. When cytoplasmic Mdm2 level gets too low to feed nuclear Mdm2, nuclear Mdm2 level then starts to decrease leading to the second fold observed in the large amplitude limit cycle in domain D^{21}. As nuclear Mdm2 level goes below its threshold K_P, nuclear Mdm2 no longer inhibit p53 activity whose level starts to increase again (domain D^{11} and D^{12}) until it reaches its threshold K_{Mc} which closes the trajectory of the large amplitude limit cycle.

The analysis of the orbits of the two oscillatory regimes thus brings out two key qualitative features which characterize the birhythmic behavior:

- the choice between two transitions when the system reaches domain D^{22} which induces a separation in the phase space between the two oscillatory regimes. This branching point gives rise to two embedded cycles in the graph showing the transitions followed by the two oscillatory regimes in the phase space (Figure 5B). This result is in accordance with the logical analysis of the p53-Mdm2 network which brought out an oscillatory regime composed of several small and large amplitude embedded cycles in the transition graph of the system (see Figure 3 in [12]);
- the presence of a “tail” containing two folds in the orbit of the high amplitude oscillatory regime (Figure 6, domain D^{21}) whose emergence can be interpreted in terms of the competition between two opposite processes: Mdm2 translocation from the cytoplasm to the nucleus on one hand and p53-mediated inhibition of Mdm2 nuclear entry on the other hand.

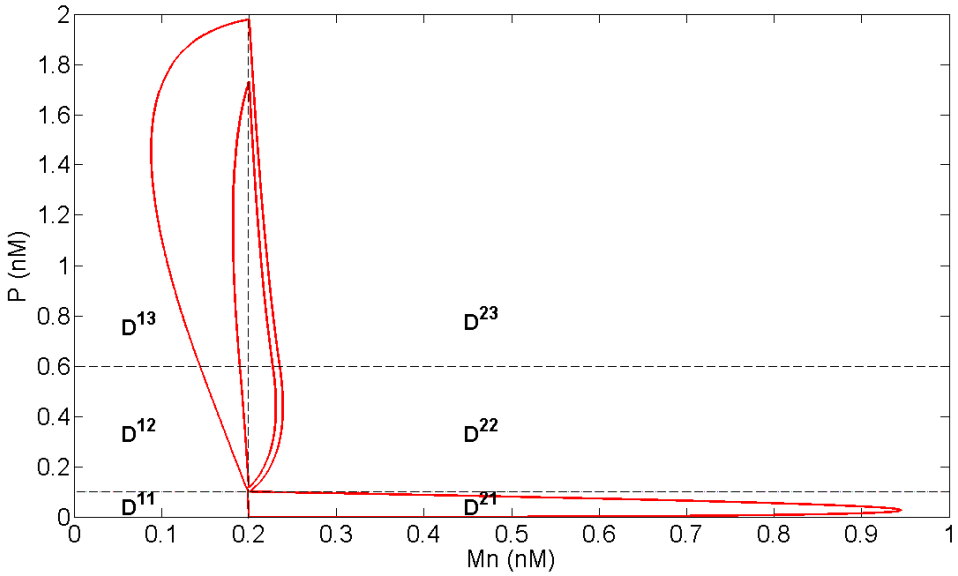


Figure 6. Projection of the phase portrait of birhythmicity in the plane (Mn,P) for Model 2. Projection of the two oscillatory regimes composing the birhythmic behavior of Model 2 in the plane (Mn,P). The dashed lines represent the thresholds of the step functions: K_{Mn} and K_{Mc} for P, K_P for Mn. The parameter values are the same as for Figure 3 (K_{Mn}=0.1 nM, K_P=0.2 nM) except K_{Mc}=0.6 nM. The period of the large amplitude oscillatory regime is significantly longer than the period of the small amplitude oscillatory regime (see Figure 8A and 8C).

2.4 Analysis of the basic mechanisms for the emergence of birhythmicity

2.4.1 A two-dimensional reduced model

In order to get more insight into the basic mechanisms leading to the birhythmicity, we looked for a further approximation of the previous 3-dimensional Model 2 which would preserve the birhythmic behavior as well as the characteristics of the orbits of the two oscillatory regimes underlined by the previous analysis. In Model 2, in each domain, the evolution of Mn depends on Mc whereas the evolution of Mc does not depend on the other variables of the system (Table S1). We thus considered Mc as a forcing external parameter applied on the evolution of Mn. In this respect, we set Mc as a constant Mc^{ij} in each domain D^{ij} of the phase space under some constraints on the Mc^{ij} values which will be detailed further.

This approximation leads to a 2-dimensional piecewise linear differential model describing our system in which, in each domain of the phase space delimited by the thresholds K_{Mc}, K_{Mn} and K_P, the evolution of each variable is of the form:

$$\frac{dx}{dt} = k_{ij} - d \cdot x$$

where x represents the level of P or Mn, k_{ij} is a constant which depends on the domain D^{ij} of the phase space and d is the degradation rate of P or Mn. This type of piecewise diagonal linear systems belongs to a class of dynamical systems proposed originally by Glass and Kaufman [29]. Interestingly, these systems have mathematical properties which favor the qualitative anal-

ysis of their dynamics [35-38]. In particular, one can derive the so-called *transition graph*, which describes all the possible transitions between the different domains, from the position of the target equilibrium points of each domain (called the *focal points*) [31,35,36, 38].

In order to reproduce the two folds forming the "tail" which characterize the large amplitude oscillatory regime of long period in Model 1 and Model 2, we added another threshold K ($K<K_{Mn}$) for p53 level. As the evolution of Mn in each domain is now monotone, the introduction of this new threshold allows changing the sign of the derivative of Mn as the system crosses threshold K and thus recovering in particular the fold observed in domain D^{21} in Model 2 (Figure 6). The space of variables can thus be decomposed into 8 domains (D^{11}, D^{21}, D^{12}, D^{22}, D^{13}, D^{23}, D^{14}, D^{24}), defined by the thresholds K_{Mc}, K_{Mn} plus the additional threshold K for p53, and K_P for nuclear Mdm2 (Figure 7). The equations of evolution in each domain of the phase space are detailed is Table S4 (Model 3).

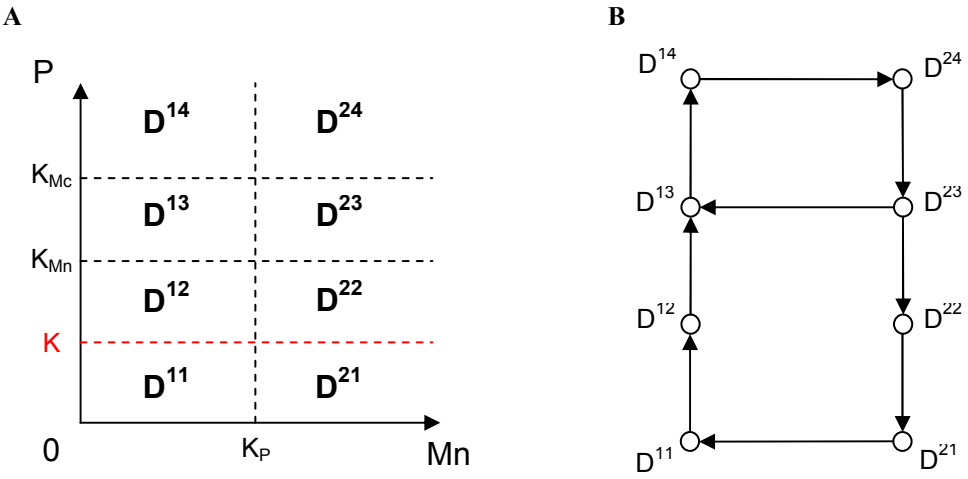


Figure 7. Subdivision of the phase space and transition graph for Model 3. (A) Subdivision of the phase space for Model 3 in 8 domains delimited by the thresholds K_P, K_{Mn}, K_{Mc} and the additional threshold K (in red). (B) Transition graph of Model 3. The graph contains two embedded cycles and a branching point in domain D^{23}. From this domain, the system can either go to domain D^{13} or domain D^{22} depending on the initial conditions.

Moreover, in order to keep the basic characteristics of the birhythmic behavior shown in Model 2, we imposed the following constraints on the parameters values of Model 3 (see Table S5 and Text S5 for more details):

- constraint (1): the transition graph of Model 3 contains the transitions between the different domains followed by the two oscillatory regimes in Model 2 (Figures 6 and 7).
- constraint (2): the setting of the parameters Mc^{ij} in each domain D^{ij} of the phase space of Model 3 has to be in accordance with the evolution of Mc in the two oscillatory regimes from one domain to another in Model 2 (Figure 8).

Finally, in order to simplify the calculation of the return map (see the following section on the analysis of the first return map), the values of the degradation rate, d_{Mn} and d_P, have been chosen to be the same. In this case, the trajectories in each domain of the phase space are straight lines, which greatly reduce the computation of the return map. However, considering different degradation rate values does not change the main results of our analysis (not shown).

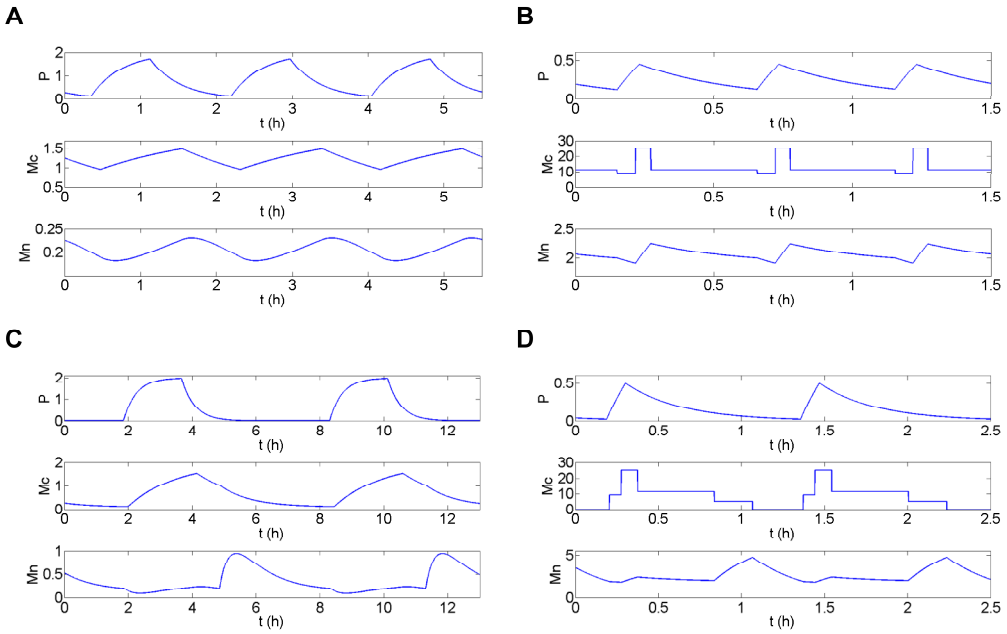


Figure 8. Temporal simulations for Model 2 and Model 3. Temporal simulation (h) of the concentration (in nM) of p53 (P), cytoplasmic Mdm2 (Mc) and nuclear Mdm2 (Mn) for Model 2 (A and C) and Model 3 (B and D) in the small amplitude short period (A and B) and the large amplitude long period (C and D) oscillatory regime. For Model 3, Mc has been set as a constant Mc^{ij} in each domain D^{ij} of the phase space delimited by the thresholds. The parameter values are indicated in Figure 6 for Model 2 and in Figure 9 for Model 3.

2.4.2 Numerical simulations of the 2-dimensional model

For appropriate parameter settings respecting the constraints stated before, numerical simulations show that the system presents a birhythmic behavior whose phase portrait is similar to the projection in the plane (Mn,P) of the phase portrait of the birhythmic behavior observed in Model 2 (Figure 9). In accordance with constraint (1), the small amplitude limit cycle crosses domains D^{14}, D^{24}, D^{23} and D^{13} whereas the large amplitude limit cycle passes through all the domains of the phase space. As shown in the transition graph, when the system reaches domain D^{23}, it can either go to D^{13} or D^{22}. This branching point thus induces a separatrix in D^{23}, passing through the threshold intersection ($Mn=K_P$, $P=K_{Mn}$) and the focal point of D^{23}, which delimits the basins of attraction of the two oscillatory regimes of the birhythmic behavior (Figure 10, blue curve). Finally, the large amplitude cycle contains a "tail" with two folds which appear at two domain transitions: D^{23} to D^{22} when the level of P crosses K_{Mn} and D^{22} to D^{21} when the level of P level crosses the additional threshold K. These folds reproduce the two folds observed in the large amplitude limit cycle in Model 2 (see Figure 6).

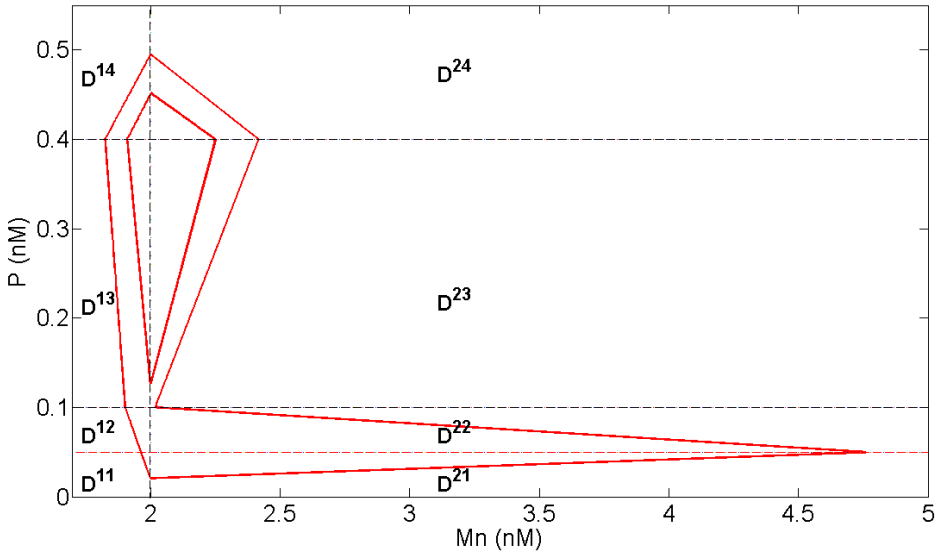


Figure 9. Phase portrait of birhythmicity for Model 3. Simulation of the two oscillatory regimes in the phase space for Model 3. The dashed lines represent the thresholds K_{Mc}, K_{Mn} and K for P, K_P for Mn. The parameter values are the same as for Figure 6 (K_{Mn}=0.1 nM) except K_{Mc}=0.4 nM , K_P=2 nM, K=0.05 nM, d_P=3 h^{-1}, Mc^{11}=Mc^{21}=Mc^{12}=0, Mc^{22}=5 nM, Mc^{13}=9 nM, Mc^{23}=11.3 nM, Mc^{14}= Mc^{24}=25 nM. Note that, since the degradation constants d_{Mn} and d_P have the same values, the trajectories in each domain are straight lines.

2.4.3 Analysis of a first return map of the 2-dimensional model

We next looked for a proof of the existence of birhythmicity by analyzing the first return map from and to the boundary between the domains D^{14} and D^{24} ([0, x) axis in Figure 10) which is crossed by both oscillatory regimes. The return map (or Poincaré map) of a surface S (here the [0, x) axis) is a mapping of S obtained by following trajectories from one intersection with S to the next [39]. This mapping is described by the equation:

$$x_{n+1} = F(x_n)$$

where x_n (resp. x_{n+1}) represents the n^{th} (resp $n+1^{th}$) intersection of the trajectory of the system with S, and F represents the return map. In this description, the periodic orbits crossing S corresponds to fixed points of function F.

Here, an analytical expression of the return map of the [0, x) axis can be calculated (see Text S6). The results of our analysis show that the return map presents two strictly positive fixed points which correspond to the two oscillatory regimes shown by the numerical simulations in Figure 9 (Figure 10B and 10D, green curve), proving the existence of birhythmicity in Model 3. Moreover and surprisingly, a discontinuity point appears which separates the [0, x) axis in two intervals: the interval [0, x_D] for which the system tends to the small amplitude oscillatory regime ($x=x_1$) (Figure 10C and 10D); the interval $x>x_D$ for which the system tends to the large amplitude oscillatory regime ($x=x_2$) (Figure 10A and 10B). For the critical point $x=x_D$, the trajectory hits the threshold intersection point (K_P, K_{Mn}) (Figure 10A and 10C, blue curve), drawing the separatrix of the system in D^{23}. Therefore, the branching point of the transition graph,

which induces this separatrix, is at the origin of the discontinuity point observed in the return map.

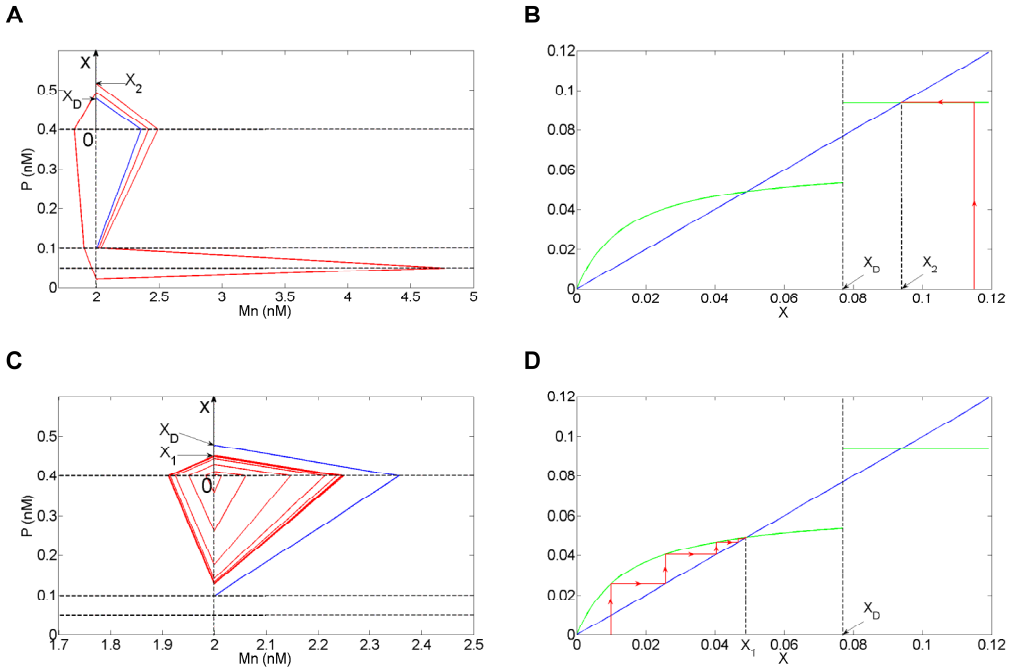


Figure 10. First return map analysis for Model 3. (A and C) In red, simulation in the phase plane for the initial conditions Mn=2 nM and P=0.515 nM ($x>x_D$, panel A) or P=0.401 nM ($x<x_D$, panel C) for Model 3. The dashed lines represent the thresholds K_{Mc}=0.4 nM, K_{Mn}=0.1 nM and K=0.05 nM for P, K_P=2nM for Mn. (B and D) In red, simulation of the orbit of the first return map from and to the [0, x) axis for the initials conditions of panel A (panel B) and panel C (panel D). The first return map F is shown in green and has been derived analytically (see Text S6). The parameter values are indicated in Figure 9. The discontinuity in F at $x=x_D$~0.077 arises when the trajectory hits the threshold intersection point (Mn=K_P=2, P=K_{Mn}=0.1) (blue curve). The fixed points of F correspond to the two limit cycles of the system shown in Figure 9. For $x>x_D$ (resp. $x<x_D$), the trajectory tends to the large (resp. small) amplitude oscillatory regime corresponding to the fixed point $x=x_2$~0.093 (resp. $x=x_1$~0.048).

We then investigated the role of the "tail" which characterizes the large amplitude oscillatory regime in the emergence of the birhythmicity by using the return map description. To do so, we suppressed this "tail", while keeping the two embedded cycles in the transition graph, by adding a transition from domain D^{22} to domain D^{12} in the transition graph (Figure 11A). We then calculated the first return map in the [0, x) axis for this modified Model 3 (see Text S6 for details of the calculation). The results show that the large amplitude limit cycle disappeared (Figure 11B). Indeed, the first return map ceases to be discontinuous and instead presents a non smooth point for the same x_D value than before (Text S6). The loss of the discontinuity point accompanies the loss of the fixed point, $x=x_2$, corresponding to the large amplitude oscillatory regime. Therefore, the "tail" is here necessary for the emergence of the birhythmic behavior. More precisely, the suppression of the "tail" leads to the disappearance of the discontinuity of

the first return map which has for consequence the disappearance of the large amplitude limit cycle.

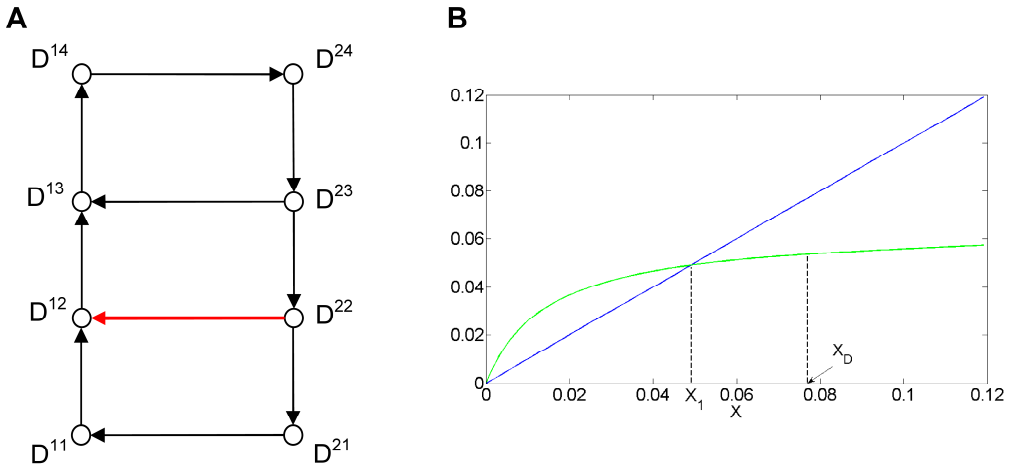


Figure 11. Transition graph and first return map for the modified Model 3. (A) Transition graph of the modified model 3. (B) Graph of the corresponding first return map (in green) from and to the [0, x) axis (see Figure 10). The parameter values are indicated in Figure 9, except $Mc^{22}=1$. The focal point of D^{22} is now in D^{11} inducing the additional transition from D^{22} to D^{12} (arrow in red). The fixed points of the first return function correspond to limit cycles of the system. The system presents a unique limit cycle ($x=x_1\sim0.048$) corresponding to the small amplitude oscillatory regime (see Figure 10). The first return map shows a non smooth point at $x_D\sim0.077$ (see Text S6).

2.4.4 An experimental strategy to reveal birhythmicity in the p53-Mdm2 network

From the previous analysis, an experimental strategy can be proposed to test the existence of the birhythmic behavior predicted by the OAK Model. The experiments performed on irradiated cells by Geva-Zatorsky et al. showed the existence of two frequencies of p53 oscillations as a function of the irradiation dose but the co-existence between these two types of oscillations for the same irradiation dose has not been firmly observed experimentally so far. The 2-dimensional piecewise linear reduced system (Model 3) provides a model of the p53-Mdm2 network from which experimental strategies can be implemented to distinguish between the existence of a single oscillatory regime (mono-rhythmicity) whose frequency increases with the irradiation dose or coexistence between two oscillatory regimes for the same irradiation dose (birhythmicity).

Looking at the phase portrait of the oscillatory regimes for Model 3 (Figure 9), it's straightforward to predict that, starting from the small amplitude limit cycle of short period, an increase in p53 concentration will lead to a shift of the system to the other oscillatory regime. Indeed, numerical simulations of this model show that applying a transitory pulse of p53 when the system oscillates in the short period oscillatory regime leads to a shift to long period oscillations (Figure 12). It has to be noted that such kinds of strategies in which a transient pulse of an inducer is applied to provoke a permanent switch from one regime to another have already been implemented to reveal bistable behavior in genetic networks [40-42]. We thus propose the following experimental test:

1- Introduce an inducible P53 gene into the cells.

2- Do a preliminary experiment: set the irradiation dose range for which most of the cells are oscillating with a high frequency.
3- Apply decreasing irradiation doses to the cells starting from the dose range previously determined.
4- For each dose, freeze the DNA repair process (so that the parameter d_{Mn} of the model remains constant) then measure the distribution of the periods of p53 and Mdm2 oscillations in the cell population.
5- Apply a transitory pulse of the inducer (which will induce a transitory expression of the inducible P53 gene) and wait until the distribution of the periods among the cell population reaches a stationary regime.
6- Has the distribution shifted to long period p53 and Mdm2 oscillations? If yes, this experimental observation is consistent with the existence of a birhythmic behavior in the system.

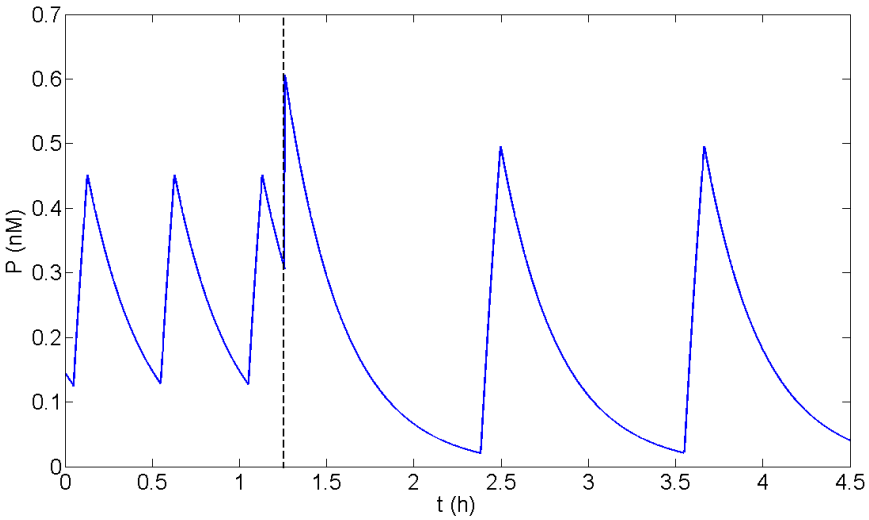


Figure 12. Permanent shift from short to long period oscillatory regime after a transient p53 pulse**.** Temporal simulation of p53 level for Model 3. A pulse of p53 is applied at t=1.2h (dashed line). Before applying the pulse, the system is oscillating in the small amplitude oscillatory regime. The p53 pulse induces a shift from the small amplitude short period to the large amplitude long period limit cycle. The parameter values are indicated in Figure 9.

3 Discussion

The specific mechanisms leading to complex dynamical behavior such as birhythmicity can be studied by approximating a model into a more qualitative system and easier to interpret reduced model while preserving the properties of interest. Following this approach, the aim of this work has been to analyze the mechanisms at the origin of the birhythmic behavior observed in Ouattara, Abou-Jaoudé and Kaufman's differential model (OAK Model) of the p53-Mdm2 network. To do so, the Hill functions have been firstly approximated into step functions leading to a 3-dimensional piecewise linear differential model in which the birhythmic behavior is conserved. An autonomous variable of the system has then been set as a constant in each domain

defined by the thresholds of the step functions, which further led to a 2-dimensional piecewise linear differential model also displaying birhythmicity.

Converting the sharp non-linearities of the model into discontinuous step functions permitted to reveal the phase space structure of the birhythmic behavior. This approximation coupled with a reduction of the dimensionality of the system, from a 3-dimensional to a 2-dimensional system by setting one variable as a constant in each domain of the phase space, then from 2-dimensional to 1-dimensional description with the use of a first return map description, further allowed us to get a reduced model from which the basic qualitative features observed in the phase space leading to birhythmicity have been extracted: (1) the presence of two embedded cycles in the transition graph of the piecewise linear models, (2) the presence of a "tail" in the orbit of the large amplitude oscillatory regime of long period.

The use of a first return map description further allowed proving the existence of birhythmicity in the framework of the 2-dimensional piecewise linear model and giving an interpretation of the role of these two features in the emergence of the birhythmic phenomenon. The analysis of the first return map showed that feature (1) was associated with a non smooth point of the return map whereas feature (2) further leads to a discontinuity in the return map, which is at the origin of the emergence of the birhythmic behavior. On a methodological level, one major advantage of this approach is to greatly facilitate the computational analysis of the model. In this regard, this method could be implemented to analyze the dynamics of other mathematical models of biological rhythms showing high enough nonlinearities.

Finally, in the light of our analysis, we proposed an experimental strategy to test the existence of birhythmicity in the p53-Mdm2 network. This strategy relies on a key characteristic of multistable systems which is to convert a transient stimulus into a permanent response of the cell. However, one may wonder what the physiological interest of birhythmicity in the p53 response to DNA damage is. One possible advantage could be to enhance the response of the system in contrast to mono-rhythmic systems which may require large perturbations and long time to induce a significant frequency change. Birhythmicity would thus allow a better flexibility of the p53 response by permitting the cell to quickly switch from one oscillatory regime to another after DNA damage.

4 Acknowledgments

The authors would like to thank Professor Marcelle Kaufman for critical reading of this report. This work was supported in part by the INRIA-INSERM initiative action ColAge.

5 Bibliography

[1]Goldbeter A (1996) Biochemical Oscillations and Cellular Rythms. The molecular basis of periodic and chaotic behavior. Cambridge University Press. 605 p.
[2]Goldbeter A (2002) Computational approaches to cellular rhythms. Nature 420(6912): 238-245.
[3]Bar-Or RL , Maya R, Segel LA, Alon U, Levine AJ et al. (2000) Generation of oscillations by the p53–mdm2 feedback loop: a theoretical and experimental study. Proc. Natl. Acad. Sci. USA 97(21): 11250–11255.
[4]Decroly O, Goldbeter A (1982) Birhythmicity, chaos, and other patterns of temporal self-organization in a multiply regulated biochemical system. Proc Natl Acad Sci U S A 79(22): 6917-6921.
[5]Alamgir M, Epstein I (1983) Birythmicity and compound oscillation in coupled chemical oscillators: chlorite-bromate-iodide system. J Am Chem Soc 105: 2500-2501.
[6]Citri O, Epstein I (1988) Mechanistic study of a coupled chemical oscillator: the bromate-chlorite-iodide reaction. Journal of Physical Chemistry 92: 1865-1871.

[7]Hounsgaard J, Hultborn H, Jespersen B, Kiehn O (1988) Bistability of alpha-motoneurones in the decerebrate cat and in the acute spinal cat after intravenous 5-hydroxytryptophan. J Physiol 405: 345-367.
[8]Ventura A, Kirsch DG, McLaughlin ME, Tuveson DA, Grimm J et al. (2007) Restoration of p53 function leads to tumour regression in vivo. Nature 445(7128): 661-665.
[9]Vogelstein B, Lane D, Levine AJ (2000) Surfing the p53 network. Nature 408(6810): 307-310.
[10]Vousden KH, Lane DP (2007) p53 in health and disease. Nat Rev Mol Cell Biol 8(4): 275-283.
[11]Geva-Zatorsky N, Rosenfeld N, Itzkovitz S, Milo R, Sigal A et al. (2006) Oscillations and variability in the p53 system. Mol Syst Biol 2.
[12]Abou-Jaoudé W, Ouattara DA, Kaufman M (2009) From structure to dynamics: frequency tuning in the p53-Mdm2 network I. Logical approach. J Theor Biol 258(4): 561-577.
[13]Ouattara DA, Abou-Jaoudé W, Kaufman M (2010) From structure to dynamics: frequency tuning in the p53-Mdm2 network. II Differential and stochastic approaches. J Theor Biol 264(4): 1177-1189.
[14]Ciliberto A, Novak B, Tyson JJ (2005) Steady states and oscillations in the p53/mdm2 network. Cell Cycle 4(3): 488-493.
[15]Brooks CL, Gu W (2006) p53 ubiquitination: Mdm2 and beyond. Mol Cell 21(3): 307-315.
[16]Fang S, Jensen JP, Ludwig RL, Vousden KH, Weissman AM (2000) Mdm2 is a RING finger-dependent ubiquitin protein ligase for itself and p53. J Biol Chem 275(12): 8945-8951.
[17]Inoue T, Geyer RK, Howard D, Yu ZK, Maki CG (2001) MDM2 can promote the ubiquitination, nuclear export, and degradation of p53 in the absence of direct binding. J Biol Chem 276(48): 45255-45260.
[18]Chen J, Lin J, Levine AJ (1995) Regulation of transcription functions of the p53 tumor suppressor by the mdm-2 oncogene. Mol Med 1(2): 142-152.
[19]Kruse J-P, Gu W (2009) Modes of p53 regulation. Cell 137(4): 609-622.
[20]Oliner JD, Pietenpol JA, Thiagalingam S, Gyuris J, Kinzler KW et al. (1993) Oncoprotein MDM2 conceals the activation domain of tumour suppressor p53. Nature 362(6423): 857-860.
[21]Barak Y, Juven T, Haffner R, Oren M (1993) Mdm2 expression is induced by wild type p53 activity. EMBO J 12(2): 461-468.
[22]Freedman DA, Wu L, Levine AJ (1999) Functions of the MDM2 oncoprotein. Cell Mol Life Sci 55(1): 96-107.
[23]Gottlieb TM, Leal JFM, Seger R, Taya Y, Oren M (2002) Cross-talk between Akt, p53 and Mdm2: possible implications for the regulation of apoptosis. Oncogene 21(8): 1299-1303.
[24]Bakkenist CJ, Kastan MB (2003) DNA damage activates ATM through intermolecular autophosphorylation and dimer dissociation. Nature 421(6922): 499-506.
[25]Stommel JM, Wahl GM (2005) A new twist in the feedback loop: stress-activated MDM2 destabilization is required for p53 activation. Cell Cycle 4(3): 411-417.
[26]Hirsch MW, Smith HL (2003) Monotone systems, a mini-review, in Positive Systems. Proceedings of the First Multidisciplinary Symposium on Positive Systems (POSTA 2003). In: Benvenuti L, De Santis A, Farina L, editors. Lecture Notes on Control and Information Sciences vol. 294. Springer Verlag, Heidelberg.
[27]Hirsch MW (1988) Systems of differential equations which are competitive or cooperative: III. Competing species. Nonlinearity 1: 51-71.
[28]Zhu H-R, Smith H (1994) Stable periodic orbits for a class of three dimensional competitive systems. J Diff Eqn 110: 143-156.
[29]Glass L, Kauffman SA (1973) The logical analysis of continuous, non-linear biochemical control networks. J Theor Biol 39(1): 103-129.
[30]Omholt SW, Kefang X, Andersen O, Plahte E (1998) Description and analysis of switchlike regulatory networks exemplified by a model of cellular iron homeostasis. J Theor Biol 195(3): 339-350.

[31]de Jong H, Gouzé J-L, Hernandez C, Page M, Sari T et al. (2004) Qualitative simulation of genetic regulatory networks using piecewise-linear models. Bull Math Biol 66(2): 301-340.
[32]Ropers D, de Jong H, Page M, Schneider D, Geiselmann J (2006) Qualitative simulation of the carbon starvation response in Escherichia coli. Biosystems 84(2): 124-152.
[33]Dayarian A, Chaves M, Sontag ED, Sengupta AM (2009) Shape, size, and robustness: feasible regions in the parameter space of biochemical networks. PLoS Comput Biol 5(1).
[34]Glass L, Pasternack JS (1978) Stable oscillations in mathematical models of biological control systems. J Math Biol 6:207-223.
[35]Snoussi E (1989) Qualitative dynamics of piecewise-linear differential equations: a discrete mapping approach. Dyn Stabil Syst 4: 189-207.
[36]Glass L (1975) Classification of biological networks by their qualitative dynamics. J Theor Biol 54(1): 85-107.
[37]Edwards R (2000) Analysis of continuous-time switching networks. Physica D 146: 165-199.
[38]Casey R, de Jong H, Gouzé, J-L (2006) Piecewise-linear models of genetic regulatory networks: equilibria and their stability. J Math Biol 52(1): 27-56.
[39]Strogatz H (1994) Nonlinear Dynamics and Chaos. With applications to Physics, Biology, Chemistry, and Engineering. Westview. 498 p.
[40]Novick A, Weiner M (1957) Enzyme induction as an all-or-none phenomenon. Proc Natl Acad Sci U S A 43(7): 553-566.
[41]Gardner TS, Cantor CR, Collins JJ (2000) Construction of a genetic toggle switch in Escherichia coli. Nature 403(6767): 339-342.
[42]Xiong W, Ferrell JE (2003) A positive-feedback-based bistable 'memory module' that governs a cell fate decision. Nature 426(6965): 460-465.

6 Supplementary materials

Text S1. The OAK Model.

We recall the differential equations which describe the model of the p53-Mdm2 core network of Ouattara et al. [1] (OAK Model):

$$\frac{\mathrm{d}P}{\mathrm{d}t} = k_P \frac{K_P^n}{K_P^n + Mn^n} - \left(d_P + d_P' Mn\right) \cdot P$$

$$\frac{\mathrm{d}Mc}{\mathrm{d}t} = k_{Mc} + k'_{Mc} \frac{P^n}{K_{Mc}^n + P^n} - \left(k_{in} - k'_{in} \frac{P^n}{K_{Mn}^n + P^n} \right) \cdot Mc + \frac{1}{V_r} k_{out} \cdot Mn - d_{Mc} Mc$$

$$\frac{\mathrm{d}Mn}{\mathrm{d}t} = V_r \left(k_{in} - k'_{in} \frac{P^n}{K_{Mn}^n + P^n} \right) \cdot Mc - k_{out} \cdot Mn - d_{Mn} Mn$$

where P, Mc and Mn represent the concentration of p53, cytoplasmic Mdm2 and nuclear Mdm2 respectively.

The terms $d_P \cdot P$ and $d_P' \cdot Mn \cdot P$ represent the basal and Mdm2-mediated degradation of p53, respectively. $k_P \frac{K_P^n}{K_P^n + Mn^n}$ refers to the production of p53. The term k_{Mc} corresponds to the basal production of Mdm2 whereas $k'_{Mc} \frac{P^n}{K_{Mc}^n + P^n}$ relates to the p53-dependent produc-

tion of cytoplasmic Mdm2. $d_{Mc}Mc$ represents the degradation of cytoplasmic Mdm2. The terms $\frac{1}{V_r}k_{out}\cdot Mn$ and $k_{out}\cdot Mn$ model the translocation process of nuclear Mdm2 into the cytoplasm whereas $\left(k_{in}-k'_{in}\frac{P^n}{K_{Mn}^n+P^n}\right)\cdot Mc$ refers to the nuclear import of cytoplasmic Mdm2 (inhibited by p53). $d_{Mn}Mn$ corresponds to the degradation of nuclear Mdm2, which is accelerated by DNA damage. Finally, Vr represents the ratio between the cytoplasmic and the nuclear volume and appears in the translocation processes involved in the model. As p53 forms a tetramer to enhance the expression of its target genes [2-4], Hill functions with exponent n=4 have been used to model the processes involving p53 activity in the OAK Model.

It should be noted that the incorporation of the nonlinear term $k_P\frac{K_P^n}{K_P^n+Mn^n}$ which models the downregulation of the production of p53 may not be fully justified on biological grounds. However, removing this term and using a nonlinear, Goldbeter–Koshland function [5] for the Mdm2-mediated degradation of p53 leads to a bifurcation picture as a function of d_{Mn} which is very similar to the bifurcation diagram of the OAK Model (see Figure A1 in [1]). Moreover, in the domain of birhythmicity, the shape of the orbits of the two limit cycles is also very similar to the one for the OAK Model (not shown).

References

[1]Ouattara DA, Abou-Jaoudé W, Kaufman M (2010) From structure to dynamics: frequency tuning in the p53-Mdm2 network. II Differential and stochastic approaches. J Theor Biol 264: 1177-1189.

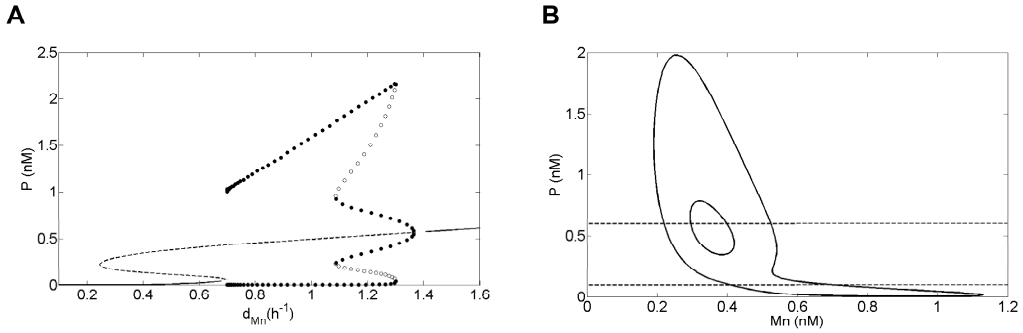
[2]Chène P (2001) The role of tetramerization in p53 function. Oncogene 20:2611-2617.

[3]McLure KG, Lee PW (1998) How p53 binds DNA as a tetramer. EMBO J 17:3342-3350.

[4]Weinberg RL, Veprintsev DB, Fersht AR (2004) Cooperative binding of tetrameric p53 to DNA. J Mol Biol 341:1145-1159.

[5]Goldbeter A, Koshland DE (1981) An amplified sensitivity arising from covalent modification in biological systems. Proc Natl Acad Sci USA 78:6840-6844.

Figure S1. Bifurcation diagram and projection of the phase portrait of birhythmicity in the plane (Mn,P) for the OAK model.



(A) Bifurcation diagrams of p53 level as a function of d_{Mn} for the OAK Model (Ouattara et al., 2010). Solid lines (resp. dashed lines) represent the stable (resp. unstable) equilibrium points. Bold (resp. white) dots are the maxima and minima of the stable (resp. unstable) limit cycles. The system shows a birhythmic domain for 1.09 h^{-1}<d_{Mn}<1.3h^{-1}. (B) Projection of the two oscillatory regimes on the plane (Mn,P) for d_{Mn}=1.2 h^{-1}. The thresholds, K_{Mc} and K_{Mn}, related to P are indicated in dashed lines. The parameter values for the bifurcation diagram are K_{Mn}=0.1 nM, K_{Mc}=0.6 nM, k_P=5 nM.h^{-1}, k_{Mc}=0.1 nM.h^{-1}, k'$_{Mc}$=1.2 nM.h^{-1}, d_P=0.1 h^{-1}, d'$_P$ = 2.3 nM^{-1}.h^{-1}, d_{Mc} = 0.6 h^{-1}, k_{in} = 0.45 h^{-1}, k'$_{in}$ = 0.4 h^{-1}, k_{out} = 0.045 h^{-1}, K_P = 0.2 nM and Vr=10.

Text S2. Estimation of the terms modeling the translocation of nuclear Mdm2 to the cytoplasm and the Mdm2-mediated acceleration of p53 degradation in the OAK Model.

a) We compared the term $k_{out} \cdot Mn$ with the other terms of the equation of evolution of Mn for the parameter values indicated in Figure S1. In the oscillatory domain (Figure S1, left), $d_{Mn} \geq 0.5h^{-1}$ and $k_{out} = 0.045h^{-1}$. The term $k_{out} \cdot Mn$ is thus small compared to the term $d_{Mn} \cdot Mn$ of the equation of Mn ($k_{out} \leq 0.1 \cdot d_{Mn}$) in the domain where the system displays oscillations. $k_{out} \cdot Mn$ is thus predicted to have little effect on the dynamics of our system in the oscillatory domain.

b) We also compared the term $\frac{1}{V_r} k_{out} \cdot Mn$ with the other terms of the equation of Mc along the orbits of the limit cycles for the parameter values indicated in Figure S1. In the oscillatory domain (Figure S1, left), we can delimit a domain in the phase space, containing the orbit of the oscillatory regimes, in which Mn<2nM (not shown). In this domain, $\frac{1}{V_r} k_{out} \cdot Mn$ ~0.01 nM.h^{-1}. This term is small compared to the basal production of Mdm2, k_{Mc} (k_{Mc}=0.1 nM.h^{-1}) suggesting that the term $\frac{1}{V_r} k_{out} \cdot Mn$ has little effect on the oscillatory dynamics of the system.

c) The inhibition of p53 by nuclear Mdm2 is modeled by two terms in the OAK Model, one of them (the Hill term $k_P \frac{K_P^4}{K_P^4 + Mn^4}$) being much more nonlinear than the other (the bilinear term $d_P' \cdot Mn \cdot P$) (see Text S1). Since the emergence of complex behaviors such as oscillations and birhythmicity is closely related to high enough nonlinearities, we predict that the bilinear term has little influence on the oscillatory dynamics of the system compared with the Hill term.

Text S3. Analytical study of Model 1.

1-Model 1 is equivalent to a competitive system

The sign of the elements of the Jacobian matrix of Model 1 is:

$$\begin{pmatrix} - & 0 & - \\ + & - & 0 \\ - & + & - \end{pmatrix}$$

After the change of variable, Mc to -Mc, the signs of the elements of the Jacobian matrix become:

$$\begin{pmatrix} - & 0 & - \\ - & - & 0 \\ - & - & - \end{pmatrix}$$

which is a competitive matrix because the off-diagonal terms of the Jacobian matrix are non positive.

2-Study of the number of equilibrium points for Model 1

The equations of Model 1 at steady state are the following:

$$(1)\ 0 = k_P \frac{K_P^4}{K_P^4 + Mn_{ss}^4} - d_P \cdot P_{ss}$$

$$(2)\ 0 = k_{Mc} + k'_{Mc} \frac{P_{ss}^4}{K_{Mc}^4 + P_{ss}^4} - \left(k_{in} - k'_{in} \frac{P_{ss}^4}{K_{Mn}^4 + P_{ss}^4} \right) \cdot Mc_{ss} - d_{Mc} Mc_{ss}$$

$$(3)\ 0 = V_r \left(k_{in} - k'_{in} \frac{P_{ss}^4}{K_{Mn}^4 + P_{ss}^4} \right) \cdot Mc_{ss} - d_{Mn} Mn_{ss}$$

where P_{SS}, Mc_{SS} and Mn_{SS} represent the steady state concentration of P, Mc and Mn respectively. The equilibrium points of Model 1 are thus the solutions of the above set of equations. We next eliminate P_{ss} and Mc_{ss} variables in order to get an equation which depends solely on Mn_{ss}. From (1), we can express P_{ss} as a function of Mn_{ss}

$$(4)\ P_{ss} = k_P \frac{K_P^4}{d_P \cdot \left(K_P^4 + {Mn_{ss}}^4\right)} = \Psi\left(Mn_{ss}\right)$$

From (3) and (4), we can express Mc_{ss} as a function of Mn_{ss}

$$(5)\ Mc_{ss} = \frac{d_{Mn}}{V_r\left(k_{in} - k'_{in}\frac{\Psi(Mn)^4}{K_{Mn}^4 + \Psi(Mn)^4}\right)} \cdot Mn_{ss}$$

By replacing Mc_{ss} and P_{ss} in (2) by their expression in (4) and (5) as functions of Mn_{ss}, we get:

(6)

$$0 = k_{Mc} + k'_{Mc}\frac{\Psi\left(Mn_{ss}\right)^4}{K_{Mc}^4 + \Psi\left(Mn_{ss}\right)^4} - \left(k_{in} - k'_{in}\frac{\Psi\left(Mn_{ss}\right)^4}{K_{Mn}^4 + \Psi\left(Mn_{ss}\right)^4}\right) \cdot \frac{d_{Mn}}{V_r\left(k_{in} - k'_{in}\frac{\Psi(Mn)^4}{K_{Mn}^4 + \Psi(Mn)^4}\right)} \cdot Mn_{ss}$$

$$- d_{Mc}\frac{d_{Mn}}{V_r\left(k_{in} - k'_{in}\frac{\Psi(Mn)^4}{K_{Mn}^4 + \Psi(Mn)^4}\right)} \cdot Mn_{ss}$$

After simplification, we finally obtain:

(7)

$$R\left(Mn_{ss}\right) = k_{Mc} + k'_{Mc}\frac{\Psi\left(Mn_{ss}\right)^4}{K_{Mc}^4 + \Psi\left(Mn_{ss}\right)^4} - \frac{d_{Mc} \cdot d_{Mn}}{V_r\left(k_{in} - k'_{in}\frac{\Psi\left(Mn_{ss}\right)^4}{K_{Mn}^4 + \Psi\left(Mn_{ss}\right)^4}\right)} \cdot Mn_{ss} - \frac{1}{V_r} d_{Mn} \cdot Mn_{ss} = 0$$

with $\Psi\left(Mn_{ss}\right) = k_P \frac{K_P^4}{d_P \cdot \left(K_P^4 + {Mn_{ss}}^4\right)}$

R(0) is positive, $\lim_{x \to +\infty} R(x) = -\infty$ and R is continuous in R^3_+. Therefore, R has at least one root in R^3_+ so at least one equilibrium point in R^3_+.

We next searched bounds for Mn_{ss} value. By multiplying the equation of evolution of cytoplasmic Mdm2 by Vr and adding it to the equation of nuclear Mdm2, we obtain:

$$\begin{aligned}\frac{\mathrm{d}\left(V_r Mc + Mn\right)}{\mathrm{d}t} &= V_r\left(k_{Mc} + k'_{Mc}\frac{P^4}{K_{Mc}^4 + P^4}\right) - V_r d_{Mc} Mc - d_{Mn} Mn \\ &\le V_r\left(k_{Mc} + k'_{Mc}\right) - \min\left(d_{Mc}, d_{Mn}\right) \cdot \left(V_r Mc + Mn\right)\end{aligned}$$

Thus, we can fix ε_0 as small as we want such that we have for t sufficiently high:

$$V_r Mc + Mn \le \frac{V_r\left(k_{Mc} + k'_{Mc}\right)}{\min\left(d_{Mc}, d_{Mn}\right)} \cdot \left(1 + \varepsilon_0\right)$$

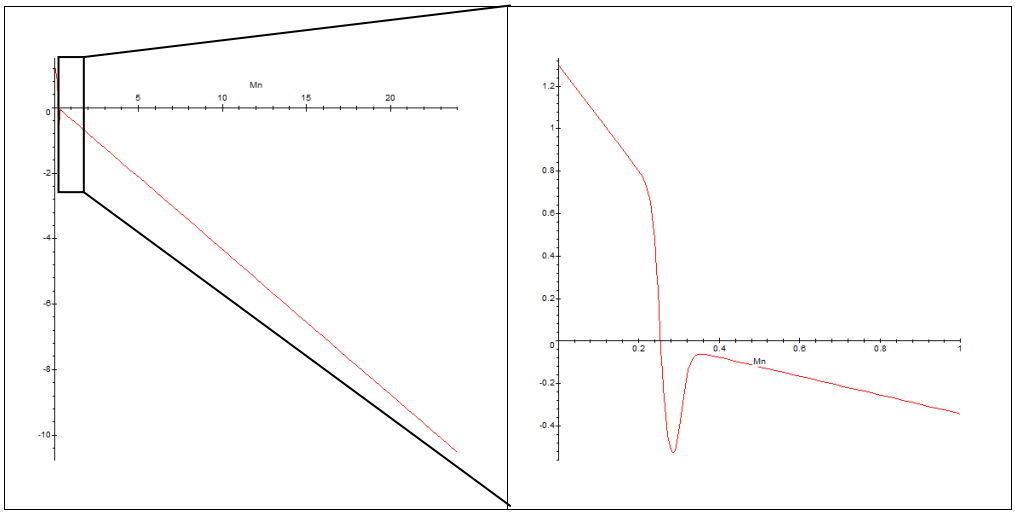
By taking for example ε_0=0.1, we obtain that the steady state of Mn, Mn_{ss}, belongs to the interval: I=[0, $1.1 \cdot \frac{V_r\left(k_{Mc}+k'_{Mc}\right)}{\min\left(d_{Mc},d_{Mn}\right)}$].

The graph of R, for the parameter values indicated in Figure 3, is presented in Figure S2. The graph shows only one zero in the interval I. Therefore, for these parameter values, Model 1 presents a unique equilibrium point.
As seen above, Model 1 is equivalent to a competitive system. Therefore, the system has one real negative eigenvalue in R^3_+ [1]. A numerical analysis further shows that, at the equilibrium point and for the parameter values indicated in Figure 3, the two other eigenvalues are complex with a positive real part (not shown). Therefore, the equilibrium point is unstable and presents a 1-dimensional stable manifold.

Reference

[1]Hirsch MW (1988) Systems of differential equations which are competitive or cooperative: III. Competing species. Nonlinearity 1:51-71.

Figure S2. Study of the number of equilibrium points for Model 1.



Graph of the rational function R (left) and a zoom of this graph (right) for the parameter values indicated in Figure 3. The roots of R give the equilibrium points for Model 1. The equilibrium points are included in the interval $[0;1.1 \cdot \frac{V_r\left(k_{Mc}+k'_{Mc}\right)}{\min\left(d_{Mc},d_{Mn}\right)} \approx 23.83]$.

Table S1. Equations of evolution for Model 2.

The domains D^{ij} of the phase space are delimited by the threshold values of the step functions: K_P, K_{Mn} and K_{Mc} (Figure 5A).

Domain D^{13} **$P>K_{Mc}$ and $Mn<K_P$**	**Domain D^{23}** **$P>K_{Mc}$ and $Mn>K_P$**
$\frac{dP}{dt} = k_P - d_P \cdot P$ $\frac{dMc}{dt} = k_{Mc} + k'_{Mc} - (k_{in} - k'_{in} + d_{Mc}) \cdot Mc$ $\frac{dMn}{dt} = V_r (k_{in} - k'_{in}) \cdot Mc - d_{Mn} Mn$	$\frac{dP}{dt} = -d_P \cdot P$ $\frac{dMc}{dt} = k_{Mc} + k'_{Mc} - (k_{in} - k'_{in} + d_{Mc}) \cdot Mc$ $\frac{dMn}{dt} = V_r (k_{in} - k'_{in}) \cdot Mc - d_{Mn} Mn$
Domain D^{12} **$K_{Mn}<P<K_{Mc}$ and $Mn<K_P$**	**Domain D^{22}** **$K_{Mn}<P<K_{Mc}$ and $Mn>K_P$**
$\frac{dP}{dt} = k_P - d_P \cdot P$ $\frac{dMc}{dt} = k_{Mc} - (k_{in} - k'_{in} + d_{Mc}) \cdot Mc$ $\frac{dMn}{dt} = V_r (k_{in} - k'_{in}) \cdot Mc - d_{Mn} Mn$	$\frac{dP}{dt} = -d_P \cdot P$ $\frac{dMc}{dt} = k_{Mc} - (k_{in} - k'_{in} + d_{Mc}) \cdot Mc$ $\frac{dMn}{dt} = V_r (k_{in} - k'_{in}) \cdot Mc - d_{Mn} Mn$
Domain D^{11} **$P<K_{Mn}$ and $Mn<K_P$**	**Domain D^{21}** **$P<K_{Mn}$ and $Mn>K_P$**
$\frac{dP}{dt} = k_P - d_P \cdot P$ $\frac{dMc}{dt} = k_{Mc} - (k_{in} + d_{Mc}) \cdot Mc$ $\frac{dMn}{dt} = V_r \cdot k_{in} \cdot Mc - d_{Mn} Mn$	$\frac{dP}{dt} = -d_P \cdot P$ $\frac{dMc}{dt} = k_{Mc} - (k_{in} + d_{Mc}) \cdot Mc$ $\frac{dMn}{dt} = V_r \cdot k_{in} \cdot Mc - d_{Mn} Mn$

Table S2. Target equilibrium points for Model 2.

In each domain D^{ij}, the equations of evolution are linear and the Jacobian matrix is triangular with negative elements in the diagonal (see Table S1). In each domain D^{ij} of the phase space, the system will thus tend towards the target equilibrium of D^{ij}.

Domain	Target equilibrium point
$\mathbf{D^{11}}$	$P^{11} = \frac{k_P}{d_P}$ $Mc^{11} = \frac{k_{Mc}}{k_{in} + d_{Mc}}$ $Mn^{11} = \frac{V_r \cdot k_{in}}{d_{Mn}} \cdot \frac{k_{Mc}}{k_{in} + d_{Mc}}$
$\mathbf{D^{21}}$	$P^{21} = 0$ $Mc^{21} = \frac{k_{Mc}}{k_{in} + d_{Mc}}$ $Mn^{21} = \frac{V_r \cdot k_{in}}{d_{Mn}} \cdot \frac{k_{Mc}}{k_{in} + d_{Mc}}$
$\mathbf{D^{12}}$	$P^{12} = \frac{k_P}{d_P}$ $Mc^{12} = \frac{k_{Mc}}{k_{in} - k'_{in} + d_{Mc}}$ $Mn^{12} = \frac{V_r\left(k_{in} - k'_{in}\right)}{d_{Mn}} \cdot \frac{k_{Mc}}{k_{in} - k'_{in} + d_{Mc}}$
$\mathbf{D^{22}}$	$P^{22} = 0$ $Mc^{22} = \frac{k_{Mc}}{k_{in} - k'_{in} + d_{Mc}}$ $Mn^{22} = \frac{V_r\left(k_{in} - k'_{in}\right)}{d_{Mn}} \cdot \frac{k_{Mc}}{k_{in} - k'_{in} + d_{Mc}}$
$\mathbf{D^{13}}$	$P^{13} = \frac{k_P}{d_P}$ $Mc^{13} = \frac{k_{Mc} + k'_{Mc}}{k_{in} - k'_{in} + d_{Mc}}$ $Mn^{13} = \frac{V_r\left(k_{in} - k'_{in}\right)}{d_{Mn}} \cdot \frac{k_{Mc} + k'_{Mc}}{k_{in} - k'_{in} + d_{Mc}}$
$\mathbf{D^{23}}$	$P^{23} = 0$ $Mc^{23} = \frac{k_{Mc} + k'_{Mc}}{k_{in} - k'_{in} + d_{Mc}}$ $Mn^{23} = \frac{V_r\left(k_{in} - k'_{in}\right)}{d_{Mn}} \cdot \frac{k_{Mc} + k'_{Mc}}{k_{in} - k'_{in} + d_{Mc}}$

Text S4. Comparison between the bifurcation diagrams of Model 1 and Model 2.

We first derive the conditions on the parameter values for Model 2 to have a stable equilibrium point in domain D^{21} (low p53 level, high nuclear Mdm2 level) and the conditions to have a stable equilibrium point in domain D^{13} (high p53 level, low nuclear Mdm2 level).
To have a stable equilibrium point in domain D^{21}, the target equilibrium point of D^{21} (Table S2) has to belong to D^{21}. This leads to the following conditions:

$$\frac{V_r \cdot k_{in}}{d_{Mn}} \cdot \frac{k_{Mc}}{k_{in} + d_{Mc}} \geq K_P \text{ which leads to } d_{Mn} \leq \frac{V_r \cdot k_{in}}{K_P} \cdot \frac{k_{Mc}}{k_{in} + d_{Mc}} = d_1$$

Similarly, to have a stable equilibrium point in domain D^{13}, the target equilibrium point of D^{13} (Table S2) has to belong to D^{13}. This leads to the following conditions:

$$\frac{k_P}{d_P} \geq K_{Mc} \text{ and } \frac{V_r\left(k_{in} - k'_{in}\right)}{d_{Mn}} \cdot \frac{k_{Mc} + k'_{Mc}}{k_{in} - k'_{in} + d_{Mc}} \leq K_P$$

which leads to :

$$\frac{k_P}{d_P} \geq K_{Mc} \text{ and } d_{Mn} \geq \frac{V_r\left(k_{in} - k'_{in}\right)}{K_P} \cdot \frac{k_{Mc} + k'_{Mc}}{k_{in} - k'_{in} + d_{Mc}} = d_2$$

For the parameter values indicated in Figure 3, the condition $\frac{k_P}{d_P} \geq K_{Mc}$ is fulfilled and $d_1<d_2$ (d_1~2.1 h^{-1} and d_2=5 h^{-1}). Therefore, for low d_{Mn} values ($d_{Mn}<d_1$), the system presents a stable equilibrium point of low level of p53. For high d_{Mn} values ($d_{Mn}>d_2$), the system presents a stable equilibrium point of high level of p53. For intermediate d_{Mn} values ($d_1<d_{Mn}<d_2$), numerical simulations shows that the system presents an oscillatory regime with a domain of birhythmicity (Figure 5). The bifurcation picture of Model 2 as a function of d_{Mn} is thus consistent with the bifurcation diagram of Model 1 (Figure 3A).

Table S3. Equations of evolution for Model 3.

The domains D^{ij} of the phase space are delimited by the threshold values of the step functions K_P, K_{Mn}, K_{Mc} and the additional threshold K. Mc has been set as a constant Mc^{ij} in each domain D^{ij}.

Domain D^{14} **$P>K_{Mc}$ and $Mn<K_P$** $\frac{dP}{dt} = k_P - d_P \cdot P$ $\frac{dMn}{dt} = V_r\left(k_{in} - k'_{in}\right)\cdot Mc^{14} - d_{Mn}Mn$	**Domain D^{24}** **$P>K_{Mc}$ and $Mn>K_P$** $\frac{dP}{dt} = -d_P \cdot P$ $\frac{dMn}{dt} = V_r\left(k_{in} - k'_{in}\right)\cdot Mc^{24} - d_{Mn}Mn$
Domain D^{13} **$K_{Mn}<P<K_{Mc}$ and $Mn<K_P$** $\frac{dP}{dt} = k_P - d_P \cdot P$ $\frac{dMn}{dt} = V_r\left(k_{in} - k'_{in}\right)\cdot Mc^{13} - d_{Mn}Mn$	**Domain D^{23}** **$K_{Mn}<P<K_{Mc}$ and $Mn>K_P$** $\frac{dP}{dt} = -d_P \cdot P$ $\frac{dMn}{dt} = V_r\left(k_{in} - k'_{in}\right)\cdot Mc^{23} - d_{Mn}Mn$
Domain D^{12} **$K<P<K_{Mn}$ and $Mn<K_P$** $\frac{dP}{dt} = k_P - d_P \cdot P$ $\frac{dMn}{dt} = V_r \cdot k_{in} \cdot Mc^{12} - d_{Mn}Mn$	**Domain D^{22}** **$K<P<K_{Mn}$ and $Mn>K_P$** $\frac{dP}{dt} = -d_P \cdot P$ $\frac{dMn}{dt} = V_r \cdot k_{in} \cdot Mc^{22} - d_{Mn}Mn$
Domain D^{11} **$P<K$ and $Mn<K_P$** $\frac{dP}{dt} = k_P - d_P \cdot P$ $\frac{dMn}{dt} = V_r \cdot k_{in} \cdot Mc^{11} - d_{Mn}Mn$	**Domain D^{21}** **$P<K$ and $Mn>K_P$** $\frac{dP}{dt} = -d_P \cdot P$ $\frac{dMn}{dt} = V_r \cdot k_{in} \cdot Mc^{21} - d_{Mn}Mn$

Table S4. Conditions on the parameter values of Model 3 to respect constraint (1).

The focal points have been chosen such that the transition graph contains the two embedded cycles composing the graph of transitions of Model 2 (Figure 6): one cycle crossing respectively domains D^{14}, D^{24}, D^{23} and D^{13}; one cycle crossing respectively domains D^{14}, D^{24}, D^{23}, D^{22}, D^{21}, D^{11}, D^{12} and D^{13} (Figure 7). The conditions on the parameter values of Model 3 to respect constraint (1) can then be directly derived.

Domain	Focal point	Conditions on the focal points to respect constraint (1)
D^{11}	$P^{11} = \frac{k_P}{d_P}$ $Mn^{11} = \frac{V_r \cdot k_{in} \cdot Mc^{11}}{d_{Mn}}$	$P^{11} \geq K$ $Mn^{11} \leq K_P$
D^{21}	$P^{21} = 0$ $Mn^{21} = \frac{V_r \cdot k_{in} \cdot Mc^{21}}{d_{Mn}}$	$P^{21} \leq K$ $Mn^{21} \leq K_P$
D^{12}	$P^{12} = \frac{k_P}{d_P}$ $Mn^{12} = \frac{V_r \cdot k_{in} \cdot Mc^{12}}{d_{Mn}}$	$P^{12} \geq K_{Mn}$ $Mn^{12} \leq K_P$
D^{22}	$P^{22} = 0$ $Mn^{22} = \frac{V_r \cdot k_{in} \cdot Mc^{22}}{d_{Mn}}$	$P^{22} \leq K$ $Mn^{22} \geq K_P$
D^{13}	$P^{13} = \frac{k_P}{d_P}$ $Mn^{13} = \frac{V_r \left(k_{in} - k'_{in}\right) \cdot Mc^{13}}{d_{Mn}}$	$P^{13} \geq K_{Mc}$ $Mn^{13} \leq K_P$
D^{23}	$P^{23} = 0$ $Mn^{23} = \frac{V_r \left(k_{in} - k'_{in}\right) \cdot Mc^{23}}{d_{Mn}}$	$P^{23} \leq K_{Mn}$ $Mn^{23} \leq K_P$
D^{14}	$P^{14} = \frac{k_P}{d_P}$ $Mn^{14} = \frac{V_r \left(k_{in} - k'_{in}\right) \cdot Mc^{14}}{d_{Mn}}$	$P^{14} \geq K_{Mc}$ $Mn^{14} \geq K_P$
D^{24}	$P^{24} = 0$ $Mn^{24} = \frac{V_r \left(k_{in} - k'_{in}\right) \cdot Mc^{24}}{d_{Mn}}$	$P^{24} \leq K_{Mc}$ $Mn^{24} \geq K_P$

Text S5. Conditions on the parameter values of Model 3 to respect constraint (2).

To respect constraint (2), Mc^{ij} values have been chosen such as:

- $Mc^{11}<Mc^{21}<Mc^{22}<Mc^{23}<Mc^{24}$ and $Mc^{24}>Mc^{14}>Mc^{13}>Mc^{12}>Mc^{11}$. For these conditions, the parameter values Mc^{ij} are in accordance with the evolution of Mc in the large amplitude limit cycle in Model 2 (Figure 8C and 8D);
- $Mc^{13}<Mc^{14}<Mc^{24}$ and $Mc^{24}>Mc^{23}>Mc^{13}$. For these conditions, the parameter values Mc^{ij} are in accordance with the evolution of Mc in the small amplitude limit cycle in Model 2 (Figure 8A and 8B).

Text S6. Analytical expression of the first return map for Model 3.

1)Derivation of the analytical expression of the first return map in the [0, x) axis for Model 3

To compute the first return map F(x) from and to the [0, x) axis (Figure 10), we consider the point $(K_P, K_{Mc}+x_0)$ with $x_0>0$ as an initial condition and compute the function $F(x_0)$ such that $(K_P, K_{Mc}+F(x_0))$ is the image of $(K_P, K_{Mc}+x_0)$ on the [0, x) axis after one cycle in the phase space.
Since the degradation constants d_{Mn} and d_P have the same values, the trajectories in each domain are straight lines containing the focal point of the domain. If the trajectory enters domain D^{ij} from a point (x_0,y_0) and if (a^{ij},b^{ij}) is the focal point of D^{ij}, then the equations of the trajectory in D^{ij} is:

$$y = \left(\frac{y_0 - b^{ij}}{x_0 - a^{ij}} \right) \cdot x + \left(\frac{b^{ij} x_0 - a^{ij} y_0}{x_0 - a^{ij}} \right) \qquad (1)$$

As the transition graph contains two embedded cycles which both cross the [0, x) axis (Figure 7), we have to compute the first return map for each of the two cycles. To derive the conditions on x_0 to follow either the small amplitude or the large amplitude cycle of the transition graph, we first have to compute the image of a point of the [0, x) axis, (K_P, x), in the half-line of equation $\{(x,y)/x>K_P, y=K_{Mc}\}$ (i.e. boundary between domains D^{23} and D^{24}) (point $(f_1(x), K_{Mc})$), and the image of the point $(f_1(x), K_{Mc})$, in the segment of equation $\{(x,y)/x=K_P, K_{Mn}<y<K_{Mc}\}$(i.e. boundary between domains D^{13} and D^{23}) (point $(K_P, f_2(f_1(x)))$). From equation (1), we obtain the analytical expression of f_1 and f_2:

$$f_1(x) = \frac{a^{24} x + K_{Mc} K_P - b^{24} K_P}{x - b^{24} + K_{Mc}} \text{ and } f_2(x) = \frac{-b^{23} x + K_P b^{23} - K_P K_{Mc} + a^{23} K_{Mc}}{-x + a^{23}}$$

which are homographic functions.

If $f_2(x)>K_{Mn}$, the trajectory will firstly cross the boundary separating D^{13} and D^{23} and will follow the small amplitude cycle in the transition graph. Otherwise, the trajectory will firstly cross the boundary separating D^{22} and D^{23} and will follow the large amplitude cycle in the transition graph. We can thus derive the conditions on x_0 to follow either the small or the large amplitude cycle:

$f_2(f_1(x_0)) > K_{Mn}$ to follow the small amplitude cycle
$f_2(f_1(x_0)) < K_{Mn}$ to follow the large amplitude cycle

Since $f_2 \circ f_1$ is a continuous and strictly decreasing function, we can define its inverse function $(f_2 \circ f_1)^{-1}$. This yields to the following conditions:

$$0 < x_0 < x_D \text{ to follow the small amplitude cycle,}$$
$$x_0 > x_D \text{ to follow the large amplitude cycle,}$$

with $x_D = (f_2 \circ f_1)^{-1}(K_{Mn}) = (f_1^{-1} \circ f_2^{-1})(K_{Mn})$. For the parameter values indicated in Figure 9, we have x_D~0.077.

For the small amplitude cycle, we can define the image of:
- a point (K_P, x), (f_3(x), K_{Mc}), for K_{Mn}<x<K_{Mc} and 0<f_3(x)< K_P
- a point (x, K_{Mc}), (K_P, f_4(x)), in the [0, x) axis for 0<x<K_P.

Similarly, for the large amplitude cycle, we can define the image of:
- a point (x, K_{Mc}), (f_5(x), K_{Mn}), for x>K_P and f_5(x)>K_P
- a point (x, K_{Mn}), (f_6(x), K), for x>K_P and f_6(x)>K_P
- a point (x, K), (K_P, f_7(x)), for x>K_P and 0<f_7(x)<K
- a point (K_P, x), (f_8(x), K), for 0<x<K and f_8(x)<K_P
- a point (x, K), (f_9(x), K_{Mn}), for 0<x<K_P and 0<f_9(x)< K_P
- a point (x, K_{Mn}), (f_{10}(x), K_{Mc}), for 0<x<K_P and 0<f_{10}(x)<K_P

From equation (1), we obtain the analytical expression of f_3, f_4, f_5, f_6, f_7, f_8, f_9, f_{10} and f_{11}:

$$f_3(x) = \frac{a^{13}x - K_{Mc}a^{13} + K_{Mc}K_p - b^{13}K_p}{x - b^{13}}$$
$$f_4(x) = \frac{b^{14}x - K_P b^{14} + K_P K_{Mc} - a^{14}K_{Mc}}{x - a^{14}}$$
$$f_5(x) = \frac{(K_{Mn} - b^{23})\cdot x - K_{Mn}a^{23} + a^{23}K_{Mc}}{K_{Mc} - b^{23}}$$
$$f_6(x) = \frac{(K - b^{22})\cdot x - Ka^{22} + a^{22}K_{Mn}}{K_{Mn} - b^{22}}$$
$$f_7(x) = \frac{-b^{21}x + K_P b^{21} - K_P K + a^{21}K}{a^{21} - x}$$
$$f_8(x) = \frac{-a^{11}x + Ka^{11} - KK_P + b^{11}K_P}{x - b^{11}}$$
$$f_9(x) = \frac{(K_{Mn} - b^{12})\cdot x - K_{Mn}a^{12} + a^{12}K}{K - b^{12}}$$
$$f_{10}(x) = \frac{(K_{Mc} - b^{13})\cdot x - K_{Mc}a^{13} + a^{13}K_{Mn}}{K_{Mn} - b^{13}}$$

Therefore, the analytical expression of the first return map, F(x), from and to the [0, x) axis is:

$$F(x) = f_4(f_3(f_2(f_1(x)))) \quad \text{for } 0 < x < x_D$$
$$F(x) = f_4(f_{10}(f_9(f_8(f_7(f_6(f_5(f_1(x)))))))) \quad \text{for } x > x_D$$

F is thus a composition of homographic functions. It is thus also a homographic function in each of the two intervals of definition. Indeed, if we compose two homographic functions, $f(x) = \frac{ax+b}{cx+d}$ and $g(x) = \frac{a'x+b'}{c'x+d'}$, we have:

$$f(g(x)) = \frac{a\frac{a'x+b'}{c'x+d'} + b}{c\frac{a'x+b'}{c'x+d'} + d} = \frac{\frac{a(a'x+b')+b(c'x+d')}{c'x+d'}}{\frac{c(a'x+b')+d(c'x+d')}{c'x+d'}}$$
$$= \frac{a(a'x+b')+b(c'x+d')}{c(a'x+b')+d(c'x+d')} = \frac{(aa'+bc')x+(ab'+bd')}{(ca'+dc')x+(cb'+dd')}$$

which is also homographic.

For the parameter values indicated in Figure 9, we obtain:

$$F(x) \approx \frac{x}{0.23 + 16 \cdot x} \quad \text{for } 0 < x < 0.077 \qquad (2)$$
$$F(x) \approx \frac{0.1 + 0.3 \cdot x}{1.1 + 2.9 \cdot x} \quad \text{for } x > 0.077 \qquad (3)$$

According to the definition of F, the fixed points of F (i.e. points x for which F(x)=x) correspond to periodic orbits of the system crossing the [0, x) axis. From equations (2) and (3), we prove that F admits two strictly positive fixed points, x_1 and x_2 (see Figure 10), with x_1~0.048 and x_2~0.093.

Calculating the left-handed and the right-handed limit of F when x tends to x_D, we get:

$$\lim_{x \to x_D^-}(F(x)) \approx 0.054 \text{ and } \lim_{x \to x_D^+}(F(x)) \approx 0.094$$

Therefore, F admits a point of discontinuity at $x=x_D$.

2)Derivation of the analytical expression of the first return map in the [0, x) axis for the modified model 3

To compute the first return function F'(x) from and to the [0, x) axis for the modified Model 3 (Figure 11), we also have to define the image of:

- a point (x, K_{Mn}), $(K_P, f_{11}(x))$, for $x>K_P$ and $K<f_{11}(x)<K_{Mn}$,
- a point (K_P, x), $(f_{12}(x), K_{Mn})$, for $K<x<K_{Mn}$ and $0<f_{12}(x)<K_P$.

in addition to the functions defined above for the calculation of the first return map, F, of Model 3.

From equation (1), we obtain:

$$f_{11}(x) = \frac{b^{22}x - K_P b^{22} + K_P K_{Mn} - a^{22} K_{Mn}}{x - a^{22}}$$
$$f_{12}(x) = \frac{a^{12}x - K_{Mn} a^{12} + K_{Mn} K_P - b^{12} K_P}{x - b^{12}}$$

As the transition graph contains now three embedded cycles each crossing the [0, x) axis (Figure 11A), we have to compute the first return map for each of the three cycles. The conditions on x_0 to follow either the small, the intermediate or the large amplitude cycle are:

$$f_2(f_1(x_0)) > K_{Mn} \text{ to follow the small amplitude cycle}$$
$$f_2(f_1(x_0)) < K_{Mn} \text{ and } f_{11}(f_5(f_1(x_0))) > K \text{ to follow the intermediate amplitude cycle}$$
$$f_{11}(f_5(f_1(x_0))) < K \text{ to follow the large amplitude cycle}$$

This yields to the following conditions:

$$0 < x_0 < x_D \text{ to follow the small amplitude cycle,}$$
$$x_D < x_0 < x_E \text{ to follow the intermediate amplitude cycle,}$$
$$x_E < x_0 \text{ to follow the large amplitude cycle,}$$

with $x_E = (f_{11} \circ f_5 \circ f_1)^{-1}(K) = (f_1^{-1} \circ f_5^{-1} \circ f_{11}^{-1})(K)$

The analytical expression of the first return map, F'(x), from and to the [0, x) axis is:

$$F'(x) = f_4(f_3(f_2(f_1(x)))) \quad \text{for } 0 < x < x_D$$
$$F'(x) = f_4(f_{10}(f_{12}(f_{11}(f_5(f_1(x)))))) \quad \text{for } x_D < x < x_E$$
$$F'(x) = f_4(f_{10}(f_9(f_8(f_7(f_6(f_5(f_1(x)))))))) \quad \text{for } x_E < x$$

For the parameter values indicated in Figure 11, we prove that F' admits only one strictly positive fixed point, x_1, (see Figure 11) with $x_1 \sim 0.048$ (results not shown).

The left-handed and the right-handed limit of F' when x tends to x_D is the same (not shown). Therefore, F' is continuous at $x=x_D$. However, calculating the left-handed and the right-handed limit of the derivative of F' when x tends to x_D for the parameter values indicated in Figure 11, we obtain:

$$\lim_{x \to x_D^-} \frac{dF}{dx}(x) \approx 0.108 \text{ and } \lim_{x \to x_D^+} \frac{dF}{dx}(x) \approx 0.105$$

The two limits are different. Therefore, F' admits a non smooth point at $x=x_D$.